ELECTROMAGNETIC PROPAGATION IN CYLINDRICAL AND CONICAL WAVEGUIDE FEEDS WITH IMPEDANCE WALLS

by

Jeffrey David Stanier

A Thesis
Presented to the University of Manitoba
in Partial Fulfillment of the
Requirements for the Degree of
Master of Science
in
Electrical Engineering

October 1986

ELECTROMAGNETIC PROPAGATION IN CYLINDRICAL AND CONICAL WAVEGUIDE FEEDS WITH IMPEDANCE WALLS

BY

JEFFREY DAVID STANIER

A thesis submitted to the Faculty of Graduate Studies of the University of Manitoba in partial fulfillment of the requirements of the degree of

MASTER OF SCIENCE

ABSTRACT

This thesis examines the use of impedance walled cylindrical and conical waveguides as feeds for prime-focus parabolic reflectors. Firstly, a review of several feeds is presented to outline the importance of feeds with low cross-polarisation. The boundary value problem is then solved for both cylindrical and conical waveguide by applying impedance boundary conditions.

The analysis of conical horns is often simplified by simulating a narrow flare-angle horn by sections of cylindrical waveguide with different radii. This simplification is sometimes applied to large flare angle horns, leading to some misconceptions. Whereas an impedance wall is sufficient to support hybrid modes in a cylindrical waveguide, it is found that the surface impedance on the wall of a dielectric lined conical horn must be tapered as a function of distance along the horn in order to satisfy the same characteristic equation as a corrugated horn. A method of achieving this impedance taper is presented as a possible means of constructing hybrid mode horns without corrugating the wall. Finally, the aperture and far-field plots of a hybrid mode conical horn are calculated and presented.

ACKNOWLEDGEMENTS

The author wishes to express his sincere appreciation to his advisor, Dr. Michael Hamid for his constant interest and support.

Thanks are also due to Mr. Atef Elsherbeni with whom much of the work on cylindrical waveguides was done.

The author wishes to acknowledge the financial assistance of the Faculty of Graduate Studies at the University of Manitoba and the Natural Sciences and Engineering Research Council who made this research possible.

Of course, thanks are also due to my family and friends for all their support.

LIST OF FIGURES

Chapter 1

Chapter 2

Chapter 3

Chapter 4

Chapter 5

Chapter 6

LIST OF TABLES

TABLE OF CONTENTS

Chapter 1 : INTRODUCTION

The advent of satellite communication systems greatly increased the need for high performance pencil-beam antennas. A large aperture is neccessary to satisfy the gain requirements of these systems. Quasi-optical antennas such as reflector and lens antennas are obvious candidates for these applications since they are structurally and conceptually simple and at the same time offer high gain. This thesis will be concerned with the feeds used for reflector type antennas; specifically with the prime-focus parabolic type as shown in Fig. 1.1.

There are two major components in reflector systems; the reflector and the feed. The reflector modifies the path of the incoming or outgoing rays so there are two focal points; one at the feed position and the other at infinity. The most important factor affecting antenna performance with regard to the reflector is the accuracy of it's shape. A very small error in the shape of the reflector results in an imprecise focal point, thereby reducing the efficiency of the antenna system. The second critical component is the performance of the feed. The radiation pattern of the feed together with the geometry of the reflector determines the illumination, polarisation purity and ultimately the efficiency of the entire system.

Together, the feed and the reflector both contribute to the polarisation properties of an antenna system. However, the reflector shape is generally chosen to satisfy specific conditions on weight, ease of production, aperture blockage and noise performance, leaving the feed design responsible for the polarisation performance. So, it can be seen that control over the radiated field from the feed is extremely important for the success of any quasi-optical antenna system.

The use of spatially orthogonal channels for microwave communication has greatly increased the need for antenna systems with a high degree of polarisation purity. An understanding of primary and secondary field patterns and their relation to the polarisation performance of the antenna system is neccessary before

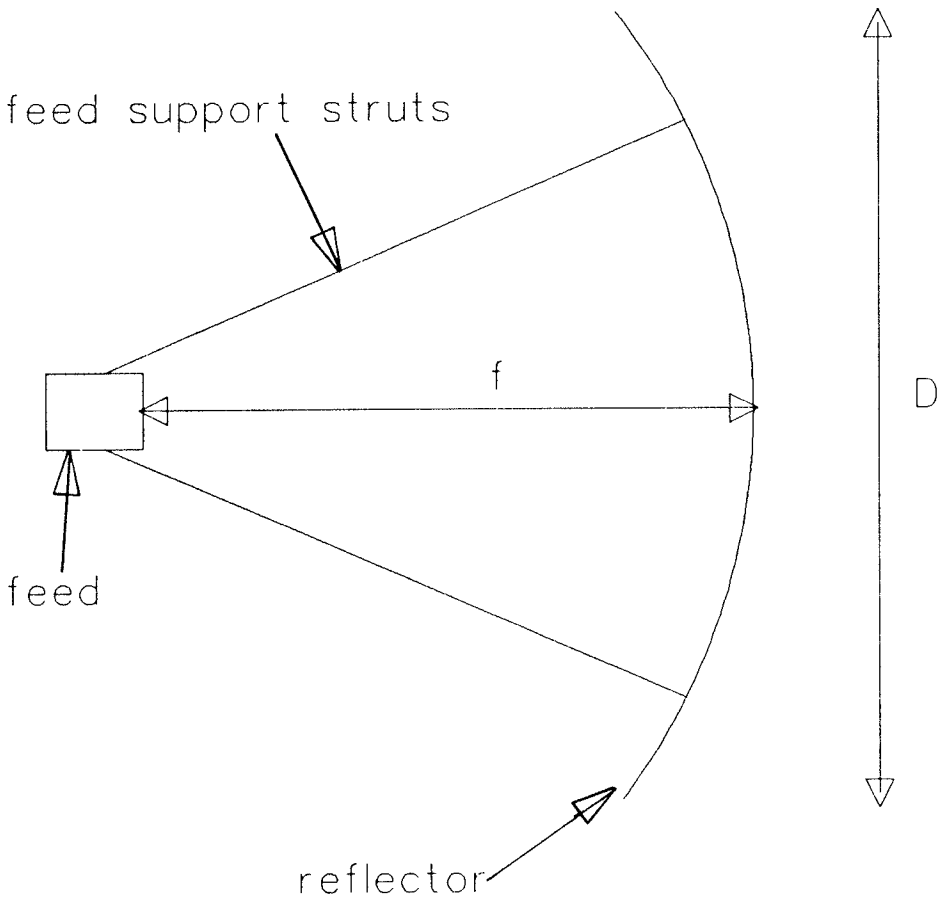

Fig. 1.1 :
Prime-Focus Reflector
Antenna System

criteria for feed design can be established.

The primary feed pattern is the radiation pattern of the horn or wire feed which is placed at the focal point of the reflector system. This pattern can be obtained from the aperture field of the feed. There are several methods for obtaining the far field of a specific aperture distribution including the equivalent source method and the Fourier transform method. Feed design is largely knowing what primary feed pattern is desirable, working backwards to the aperture field distribution and then trying to obtain this distribution by modifying the feed structure.

If the E and H-plane primary patterns are equal then there will be no cross-polarised surface currents on the reflector and the secondary pattern will be linearily polarised according to the third definition of polarization given by Ludwig [1973]. This gives us an insight into some of the characteristics of an ideal feed for a prime-focus parabaloid reflector antenna system.

The definition of cross- polarisation used most commonly for aperture antennas is Ludwig's third definition [Ludwig 1973]. This corresponds to the standard cross-polar antenna measurment set-up. The definition for the co-polar and cross-polar field vectors under this definition are;

$$a_{co} = a_\theta \cos(\phi - \phi_o) - a_\phi \sin(\phi - \phi_o)$$

$$a_x = a_\theta \sin(\phi - \phi_o) - a_\phi \cos(\phi - \phi_o)$$

where a_θ and a_ϕ are unit vectors in the spherical coordinate system and ϕ_0 is the inclination of the reference polarisation with respect to the x-axis. One major advantage of using this definition of polarisation is that a purely polarised primary pattern will tend to produce a purely polarised secondary pattern in spite of the reflector. The three conditions under which this effect is true are that;

1. the patterns of the feed and the reflector share a common central axis,
2. the reflector does not focus the far field to a point, and
3. the feed focal area should be a single point.

It can be reasoned from the above points that offset and dual reflecting antenna systems will not preserve the polarity of a purely polarised primary feed. The standard parabolic reflector in a prime focus configuration does however satisfy these conditions. For this reason this discussion will deal exclusively with feeds which are used in systems which require a purely polarised primary pattern. Multimode horns can, of course, be used in systems which require any arbitrary aperture field distribution. The problem then becomes one of discovering the optimum aperture distribution for a given reflector configuration.

Chapter 2 is a review of the feed designs presently used for prime-focus parabolic reflecting antennas. Chapter 3 of this thesis deals with the propagation of waves in a circular cylindrical waveguide when impedance boundary conditions are applied at the walls. Chapter 4 is a similar study of the conical waveguide. Both of these chapters are useful in understanding the theory behind feeds with a highly polarised aperture distribution. In chapter 4, conditions on the wall impedance of a conical horn are presented which could cause a horn to support hybrid modes without being corrugated. This idea is expanded in chapter 5 where a horn design is presented which could satisfy these impedance conditions. Chapter 6 presents aperture distributon plots of the first three HE_{1n} and EH_{1n} modes in a large conical horn. In the second part of the chapter the far field of the same six hybrid modes are calculated and presented as well as some comparisons with previously published results. The conclusions are presented in chapter 7.

Chapter 2 : PROGRESSION OF FEED DESIGNS

As we have seen, one of the most important components of a reflecting antenna system is the feed. There are several feed types which can be used successfully with parabolic reflectors, however, it is important that the proper feed is chosen to match the level of performance needed. This section briefly outlines the characteristics and performance of several popular feeds in order to highlight the role of the hybrid-mode horn.

2.1 Dipole Sources

Dipoles are seldom used as feeds in reflector systems due mainly to their poor directivity. However, an investigation of a system which uses an idealized dipole as a feed provides some useful information about the optimum characteristics of an aperture feed.

Assume a parabolic reflector with a focal axis lying along the z-axis. If a short dipole is placed at the focus of a parabolic reflector with the dipole parallel to the x-axis, there would be considerable cross-polarisation in the aperture of the paraboloid and therefore in the far field. The field distribution in the aperture of the paraboloid is shown in Fig. 2.1a. This pattern can be improved by placing a flat reflector at a distance of one-half wavelength behind the dipole, however, even this feed is poorly suited for use with a circular paraboloid since the taper is not equal in both planes.

A magnetic dipole oriented along the y-axis of the same paraboloid yields an aperture field distribution as shown in Fig. 2.1b. It is readily seen from both figures that a combination of these two distributions in the correct phase and amplitude would lead to a linearly polarised aperture field distribution, as shown in Fig. 2.1c. Jones [1954], discovered that the optimum ratio of magnetic to electric currents in the dipoles was approximately 377, the impedance of free-space.

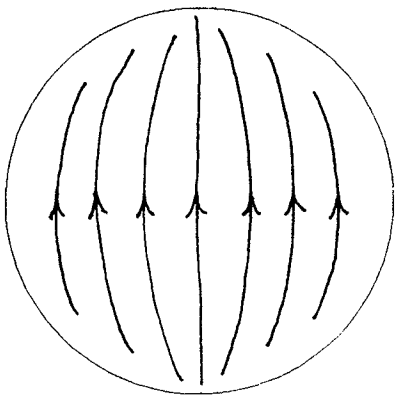

a) electric

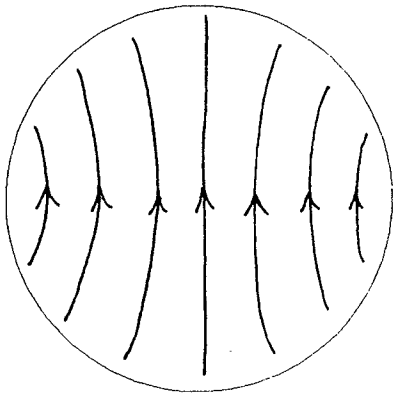

b) magnetic

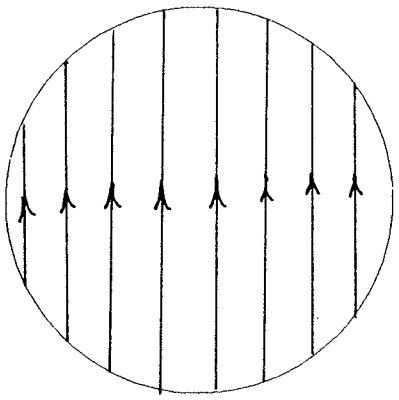

c) combined

Fig. 2.1 :
Field Patterns of a short electric and magnetic dipole

A source which displays this circular symmetry using an orthogonal pair of electric and magnetic dipoles is called a Huygen's source since it closely resembles a free-space source.

When a Huygen's source is used as a primary feed for a reflector with $\frac{f}{D}$=0.25, there would result a -12 dB illumination taper [Rudge et al 1982]. If this reflector is 25λ in diameter, the cross-polarisation level due to the axial currents on the reflector will be -44 dB. This theoretical limit to the performance of a reflector antenna can be reduced by increasing the $\frac{f}{D}$ ratio of the reflector.

Although practical dipole feeds are interesting in themselves, this thesis will not discuss them further except to say that the combining of electric and magnetic dipoles suggests the use of multimoded horns as we shall see in the next section.

2.2 Horn and Waveguide Feeds

One of the simplest feeds is an open ended rectangular waveguide or small pyramidal horn operating in the TE_{01} mode. One drawback of this type of feed is that it can only be used for linear polarisation. The dimensions of any feed with a rectangular aperture can be optimized by field matching at the aperture of the feed [Rudge and Withers 1970]. By assuming a linearly polarised plane wave incident on the reflector surface and calculating the field across an imaginary aperture at the focus, the feed may be matched to the reflector for any $\frac{f}{D}$ ratio.

Rectangular feeds are best suited for linearly polarised systems but for dual or circularly polarised systems the circular waveguide or conical horn is more useful. This is due mainly to the symmetry inherent in a circular aperture. The radiation from a circular waveguide can be calculated exactly, and thus it is possible to find the theoretical performance of an open ended cylindrical waveguide [Collin 1985]. While operating in the TE_{11} mode, and for waveguide diameters

between $0.8\lambda_0$ and $1.12\lambda_0$ the cross-polarised field in the $\phi=45^0$ plane remains below 30 dB [Collin 1985].

2.3 Multimode Horn Feeds

In the same way that the electric and magnetic dipoles can be combined to yield a linearily polarised radiated field, the modes inside a waveguide can be combined to improve the cross-polarisation performance of a waveguide or horn feed. Any combination of modes will satisfy the boundary conditions and, since the modal vectors are a complete orthogonal set of solutions to the wave equation, virtually any arbitrary aperture field may be synthesised by combining enough modes in the proper amplitude and phase.

Potter was the first to use a multimode horn to obtain a prescribed aperture field. In the Potter horn [1963], the TM_{11} mode was added in the proper phase with the TE_{11} mode to obtain a linear aperture field with equal E and H - plane radiation patterns. As was described in the introduction, these conditions are neccessary if the antenna system is to have a low cross-polarised component.

In the Potter horn the mode conversion was accomplished by a rapid change in the radius of a cylindrical waveguide, as is shown in Fig. 2.2. After a phase matching section of cylindrical waveguide, the horn then flares toward the aperture. The phase matching section is neccessary so that the two modes add with the correct phase at the aperture. In the paper by Potter [1963], the cross-polarised component in the worst case (H-plane) was -27 dB. No bandwidth information is given for this horn, and the above quoted cross-polarisation performance is at the design frequency. An additional advantage of this horn is that the phase centers in the two principle planes are at the same point.

Turrin [1969] presented another, more simple design which facilitates mode conversion by making an abrupt junction at the throat area of a conical horn, as

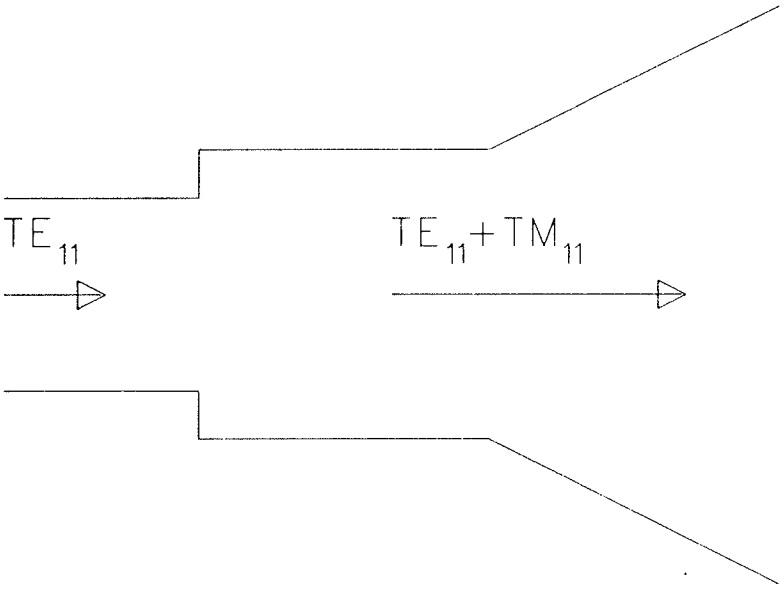

Fig. 2.2 :
The Potter Horn :
A Dual-mode Design

shown in Fig. 2.3. In this case the length of the hood (l) is chosen so the spherical modes generated at the throat add with the correct phase at the aperture. In this case the optimum ratio of TM_{11} to TE_{11} content is calculated to cancel the electric field at the wall of the the horn, a different condition than that used by Potter. This dual-mode horn developed by Turrin therefore does not have equal aperture field distributions in the E and H planes.

Another simple method of obtaining a dual mode feed is to excite the TM_{11} mode with an internal bifurcation junction as was done by Collin and Schilling [Collin 1985]. This design depends on the distance between the aperture and the internal waveguide to obtain the correct addition of the two modes at the aperture. This horn is illustrated in Fig. 2.4.

All of the above structures are inherently narrow-band structures since the aperture field is dependent on the electrical length of the waveguide between the mode converter and the aperture. There have been several attempts at increasing the bandwidth of multi-mode feeds by utilizing dielectric discontinuities in the mode-conversion structures.

One method of broad-banding the mode converter in a cylindrical waveguide was developed by Agarwal and Nagelberg [1970]. This device used a dielectric ring made of polystyrene at the discontinuity as shown in Fig. 2.5. The mode transducer was tested over a 26% bandwidth, however, no estimate was given as to how much of that bandwidth is useful.

Another simple and effective dual mode horn was developed by Satoh [1972], shown in Fig. 2.6. The Satoh horn uses a dielectric ring mounted at a stategic place on the walls of a conical horn. A bandwidth of 10% is claimed and this extended bandwidth is attributed to the use of a dielectric ring instead of a metallic discontinuity.

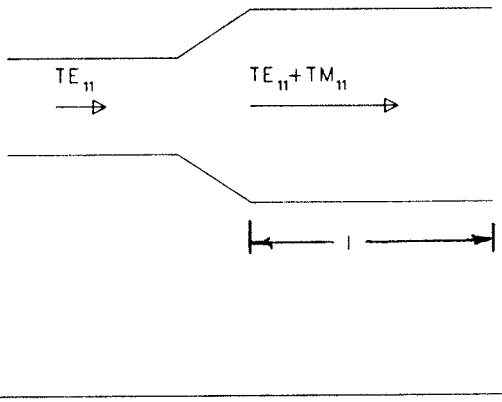

Fig. 2.3 :
A Dual-mode horn
design by Turrin

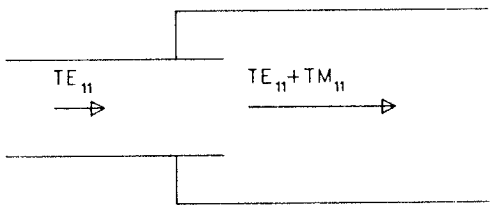

Fig. 2.4 :
A Dual-mode horn design
by Collin and Schilling

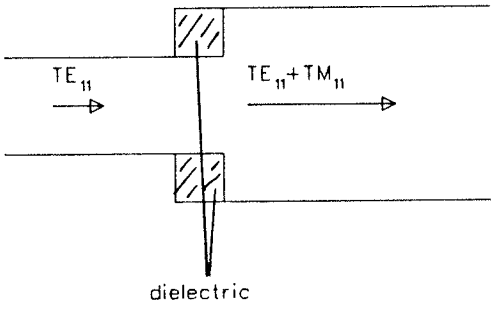

Fig. 2.5 :
A Dual-mode horn design
by Agarwal and Nagelberg

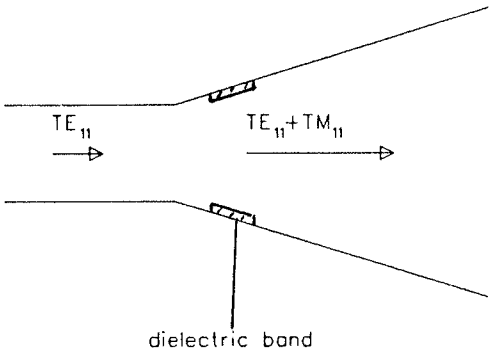

Fig. 2.6 :
A Dual-mode horn design
by Satoh

A recent extension of the Satoh horn has been developed by Wong involving concentric dielectric rings placed in a conical horn [Wong and Brandt, 1979]. Wong claims that this double ringed horn has a bandwidth greater than that of the Satoh horn as well as improved matching.

The major disadvantage of multimode feeds is that the relative phase of the constituent modes at the aperture is highly frequency dependent and this drastically degrades the performance of these horns in wide bandwidth applications. This disadvantage is partially overcome by using dielectric inserts in the feed to extend the bandwidth.

2.4 Hybrid Mode Feeds

Although improved antenna efficiency and reduced spillover were originally the impetus for developing hybrid mode feeds, the inherent symmetry and polarisation purity of the aperture field surpass that obtainable for standard horns or waveguides. There is also the added benefit of a much greater bandwidth with hybrid mode feeds than with dual mode feeds.

There are several structures which have been found to support hybrid modes. These structures include the dielectric-loaded circular waveguide [Clarricoats and Taylor 1964], the corrugated waveguide or horn [Clarricoats and Olver 1984], the dielguide [Clarricoats and Salema 1973], the dielectric filled conical horn [Lier 1986], and the large diameter waveguide with impedance walls [Dragone 1981]. This thesis presents yet another structure which could support hybrid modes [Stanier and Hamid 1986].

The basic reason that hybrid mode waveguides are useful as feeds for parabolic reflecting antennas is that the fundamental hybrid mode , the balanced HE_{11} mode, has a nearly linear aperture distribution. Fig. 2.7 displays the lines of electric field of the HE_{11} mode. This linear field distribution is very similar to that of

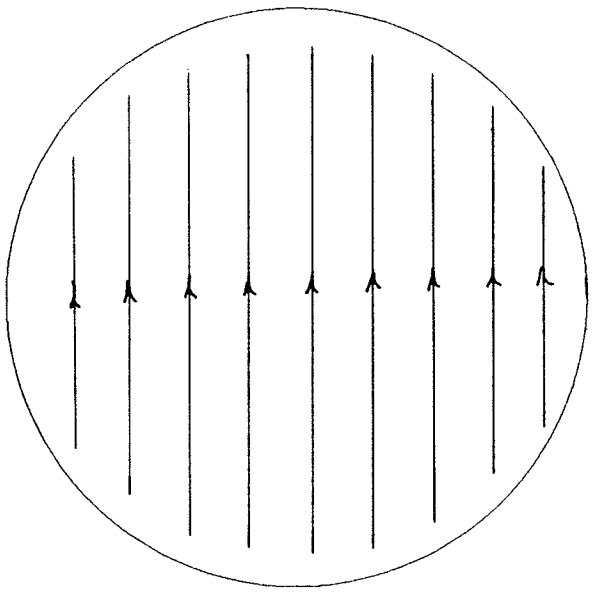

Fig. 2.7 :
Aperture field distribution of the balanced fundamental hybrid mode

the dual-mode feeds described in the last section. The major advantage of a hybrid mode horn is that the TE_{11} and the TM_{11} components of the fundamental mode satisfy the same boundary conditions and thus travel together in the waveguide. This means that the two components will be coupled together everywhere in the waveguide regardless of the frequency or length of the horn. The analysis of hybrid modes in conical structures is presented in sections 4.3 and 4.4.

One of the earliest investigations of hybrid-mode devices was by Clarricoats and Taylor [1964]. It was found that complex hybrid-modes exist in dielectric loaded circular waveguides. In that case, the loading was a rod of dielectric in the center of the waveguide.

In the early 1960's, the search for high performance horn feeds spawned what is now known as the corrugated horn. The scalar horn, as it was then termed, was first investigated by Kay [1964] and Simmons and Kay [1966]. At about the same time others were investigating similar structures [Lawrie and Peters 1966],[Minnett and Thomas 1966]. In the paper by Minnett and Thomas [1966], some theory is presented which clearly outlines the concept of TE and TM components combining into a single hybrid mode. The fundamental hybrid mode is then presented as forming a linearly polarised aperture field with equal E and H plane radiation patterns. In a companion paper by Rumsey [1966] it is further stressed that the reason for the coupling of the two component modes is that both the TE and TM modes are forced to satisfy the same boundary conditions at the wall. Fig. 2.8 shows the basic structure of a corrugated horn.

It was claimed that corrugated horns performed well over nearly an octave [Simmons and Kay 1966],[Lawrie and Peters 1966], which was signifigantly better than the multi-mode horn.

In 1969, Clarricoats analysed the corrugated horn using a spherical modal expansion [Clarricoats 1969]. In that paper, the hybridicity factor was introduced

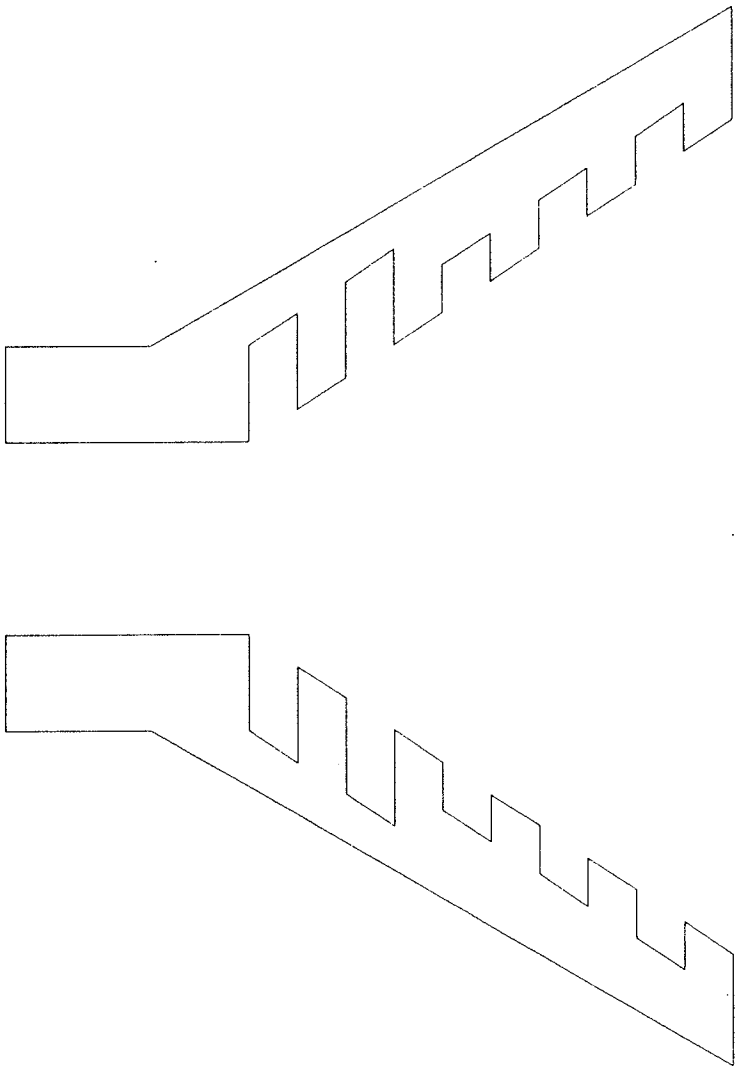

Fig. 2.8 :

The Corrugated Horn

as a measure of the relative strengths of the *TE* and *TM* components of an *HE* mode. Clarricoats also showed good agreement with the experimental results obtained by Kay. The many subsequent papers written by Clarricoats and his collegues are presented in an excellent book by Clarricoats and Olver [1984].

Experimental results were published by Jeuken [1969] and Jeuken and Lambrechtse [1969] which showed that the bandwidth of a corrugated conical horn was about 1:1.3 ; considerably less than what others had claimed. It is presently considered that the useful bandwidth of these devices is about 1:1.25 [Love 1986].

In an attempt to simplify the analysis of corrugated horns, Narasimhan [1970] used a Bessel function approximation for the θ dependence of the fields inside a conical horn. This approximation , known as McDonald's formula, is extremely useful since the more complicated Associated Legendre functions no longer have to be calculated. Although this approximation is strictly valid only for small flare angles, Narasimhan [1970] shows that it is accurate up to a flare semi-angle of 30^0. A more complete analysis of this approximation is given by Narasimhan and Rao [1969].

The analysis which has been done on dielectric loaded conical waveguide to date has treated the problem from several different viewpoints. The investigators include Felson [1959], Bahar [1967], Hamid et al. [969], Dragone [1980], Clarricoats and Salema [1973], Lier [1986] and Hadidi [1985].

Felson [1959] analysed conical and wedge shaped structures with surface impedances and showed that by linearily varying the surface impedance the boundary value problem can be simplified.

Dragone [1980,1981] has presented the analysis of hybrid modes in large diameter conical waveguide with a finite surface impedance on the wall. This analysis is applicable only to waveguides with a small flare-angle only since the waveguide is treated as a cylindrical waveguide with a slowly varying cross-section.

Of particular interest in these papers is the labelling of the two types of hybrid modes which are present in these structures. The method presented by Dragone depends on the fields approaching zero in the limit as $\theta \rightarrow \theta_1$; where θ_1 is the half-flare angle of the horn. This precludes the *EH* modes presented in the analysis by Clarricoats [1969] since these modes have maximums at the walls of the horn. Dragone calls the standard *EH* modes 'surface waves'. This thesis has adopted the terminology proposed by Clarricoats since this corresponds to the corrugated waveguide case.

Clarricoats and Salema [1973a,b] have analysed the solid dielectric conical waveguide called the 'dielguide'. This structure has been found to support hybrid modes similar to those in corrugated conical waveguide.

Another dielectric structure found to support spherical hybrid modes is the 'dual cone' structure investigated by Lier [1986]. This structure is similar to the dielguide except that on the outside wall of the dielectric cone a layer of lower permittivity, constant- thickness dielectric is placed between the outer wall of the central dielectric and the inner metal surface of the conical horn. The theory presented is based on circular waveguide analysis and tested experimentally using a narrow flare-angle horn. By assuming a long narrow horn, the dependance of the eigenvalue on the radial distance is neglected and a constant thickness gap is sufficient to support hybrid modes. This design is shown in Fig. 2.9.

Recently, the analysis of a conical horn with an arbitrary wall impedance has been published [Knop, Cheng and Ostertag 1986]. The analysis is restricted to both the area of the cone well away from the apex and to narrow flare-angles. Under these conditions, the horn almost becomes an oversized circular waveguide and not a conical horn.

Another recent investigation of a dielectric-lined conical horn by Rao is a theoretical analysis of the dual-mode horn developed by Satoh [Rao 1986],[Satoh

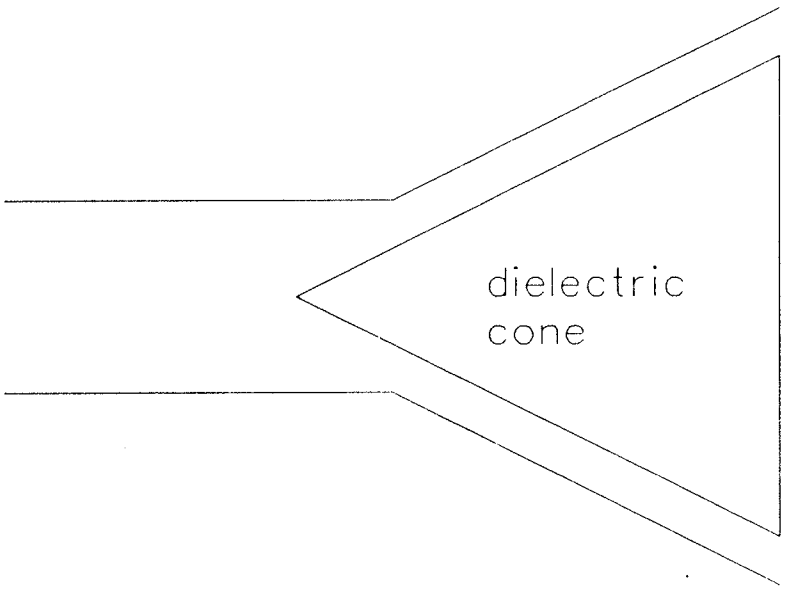

Fig. 2.9 :
A Hybrid-mode horn
design by Lier

1972]. The dielectric region is assumed to propagate hybrid modes and mode matching is applied at both ends of this region to determine the relative amplitudes of the TE_{11} and TM_{11} modes at the aperture. A major part of the analysis is to solve the boundary value problem for a dielectric lined conical waveguide by assuming a field in both the dielectric and the air regions and applying the boundary conditions at the wall and the air-dielectric interface. Unfortunately, the analysis neglects the radial dependance of the fields by using the far-field approximation. A second simplification is to assume that only the fundamental hybrid mode is propagating in the waveguide.

It can be seen from the above discussion that most of the work done on diectric lined conical horns has used the small flare angle approximation. This thesis avoids this approximation in an attempt to clarify the conditions neccessary for the propagation of hybrid modes in conical horns.

Chapter 3 : THE BOUNDARY VALUE PROBLEM FOR CYLINDRICAL STRUCTURES

3.1 Surface Impedance Boundary Conditions

The idea of using surface impedance boundary conditions was first credited to Leontovich. The boundary condition, for a surface with a finite surface impedance is given by [Senior 1962,Leontovich 1948] ;

$$\bar{E} - (\hat{n}\cdot\bar{E})\,\hat{n} = \eta_0\eta_z\,(\hat{n}\times\bar{H}) \tag{3.1.1}$$

where $\hat{n}$ is the unit outward normal at the surface and η_0, the impedance of free space. Eq. (3.1.1) is valid for any surface with a radius of curvature which is large compared to the wavelength [Senior 1962].

For a circular cylindrical waveguide with radius a the boundary conditions on the inner wall are given in circular cylindrical coordinates by

$$E_z = -\eta_z\,\eta_0\,H_\phi \quad , \; r=a \tag{3.1.2}$$

$$E_\phi = \eta_\phi\,\eta_0\,H_z \quad , \; r=a \tag{3.1.3}$$

where η_z and η_ϕ are the relative wall impedances in the $\hat{z}$ and $\hat{\phi}$ directions, respectively, and $\eta_0=(\frac{\mu_0}{\epsilon_0})^{1/2}$ is the intrinsic impedance of free space.

Expanding Eq. (3.1.1) in spherical coordinates and assuming a conical geometry yields;

$$E_R = -\eta_R\,\eta_0\,H_\phi \;\text{ and }\; E_\phi=\eta_\phi\,\eta_0\,H_R \;\; at \;\; \theta=\theta_1 \tag{3.1.4}$$

These expressions for the boundary conditions have been used in the analysis of both cylindrical and the conical waveguides in this thesis.

The concept of using impedance surfaces to simplify boundary value problems is not strictly valid as described by Waldron [1969]. In general, a surface

impedance is used to model a lossy dielectric, a dielectric coating or a corrugated surface. The impedance boundary conditions are used to simplify the geometry of the surface so it is more easily described within a specific coordinate system. For instance, a corrugated surface cannot be conveniently included in a boundary value problem since the surface cannot fit into any coordinate system. By modelling the corrugated surface as an impedance surface, the problem can then be solved. The objection raised by Waldron [1969] is that without solving the original boundary value problem exactly, we can only guess at the equivalent surface impedance of a corrugated surface in any geometrical shape. So, in order to apply the impedance boundary conditions we must first solve the exact boundary value problem and, once solved, we no longer need to use the impedance boundary conditions since we have solved the problem exactly.

Although the validity of the solution of boundary-value problems using surface impedance concepts has been criticized, such solutions have been successfully used for circular cylindrical waveguides by several authors [Mohsen and Hamid 1970],[Dragone 1981],[Lier 1986]. The use of this concept greatly simplifies the solution and allows the fields in the waveguide to be expressed in a simple form for easy comparison with other types of circular waveguides.

Previous investigators, using perturbation techniques, have found that hybrid modes can propagate in cylindrical waveguides [Papadopoulos 1954],[Karbowiak 1955]. However, their analysis is only valid for wall impedances which are nearly zero. The present analysis extends the concept to arbitrary wall impedances. Dragone [1981] has analysed circular cylindrical waveguide and established the existance of hybrid modes for non-zero wall impedances. The same conclusion is reached in this paper using a more basic approach and the concept is extended to several types of cylindrical structures including smooth-walled, corrugated, and impedance-walled waveguides.

3.2 Solution of the General Boundary Value Problem

Using the cylindrical coordinates (r, ϕ, z) and assuming an $e^{-j\omega t}$ time dependence, the fields in a circular cylindrical waveguide can be written as a combination of TE and TM components in the form [Harrington 1961]

$$E_z = (k^2 - k_z^2)\,\psi^e \tag{3.2.1}$$

$$E_\phi = j\left(\frac{k_z}{r}\right)\left(\frac{\partial \psi^e}{\partial \phi}\right) - j\omega\mu_0\left(\frac{\partial \psi^m}{\partial r}\right) \tag{3.2.2}$$

$$E_r = jk_z\left(\frac{\partial \psi^e}{\partial r}\right) + j\left(\frac{\omega\mu_0}{r}\right)\left(\frac{\partial \psi^m}{\partial \phi}\right) \tag{3.2.3}$$

$$H_z = (k^2 - k_z^2)\,\psi^m \tag{3.2.4}$$

$$H_\phi = j\left(\frac{k_z}{r}\right)\left(\frac{\partial \psi^m}{\partial \phi}\right) + j\omega\epsilon_0\left(\frac{\partial \psi^e}{\partial r}\right) \tag{3.2.5}$$

$$H_r = jk_z\left(\frac{\partial \psi^m}{\partial r}\right) - j\left(\frac{\omega\epsilon_0}{r}\right)\left(\frac{\partial \psi^e}{\partial \phi}\right) \tag{3.2.6}$$

where ψ^e and ψ^m are the scalar electric and magnetic potentials, μ_0 and ϵ_0 are the permeability and permittivity of free space respectively, ω is the angular frequency, k_z the propagation constant in the $\hat{z}$ direction and k the free space wavenumber. The coordinate system is shown in Fig. 3.1.

Substituting the field components into Eqs. (3.1.2) and (3.1.3) leads to

$$(k^2 - k_z^2)\psi_n^e = -\eta_z\,\eta_0\left[j\omega\epsilon_0\left(\frac{\partial \psi_n^e}{\partial r}\right) + j\left(\frac{k_z}{r}\right)\left(\frac{\partial \psi_n^m}{\partial \phi}\right)\right], \quad r = a \tag{3.2.9}$$

$$(k^2 - k_z^2)\psi_n^m = \frac{1}{\eta_\phi\,\eta_0}\left[j\left(\frac{k_z}{r}\right)\left(\frac{\partial \psi_n^e}{\partial \phi}\right) - j\omega\mu_0\left(\frac{\partial \psi_n^m}{\partial r}\right)\right], \quad r = a \tag{3.2.10}$$

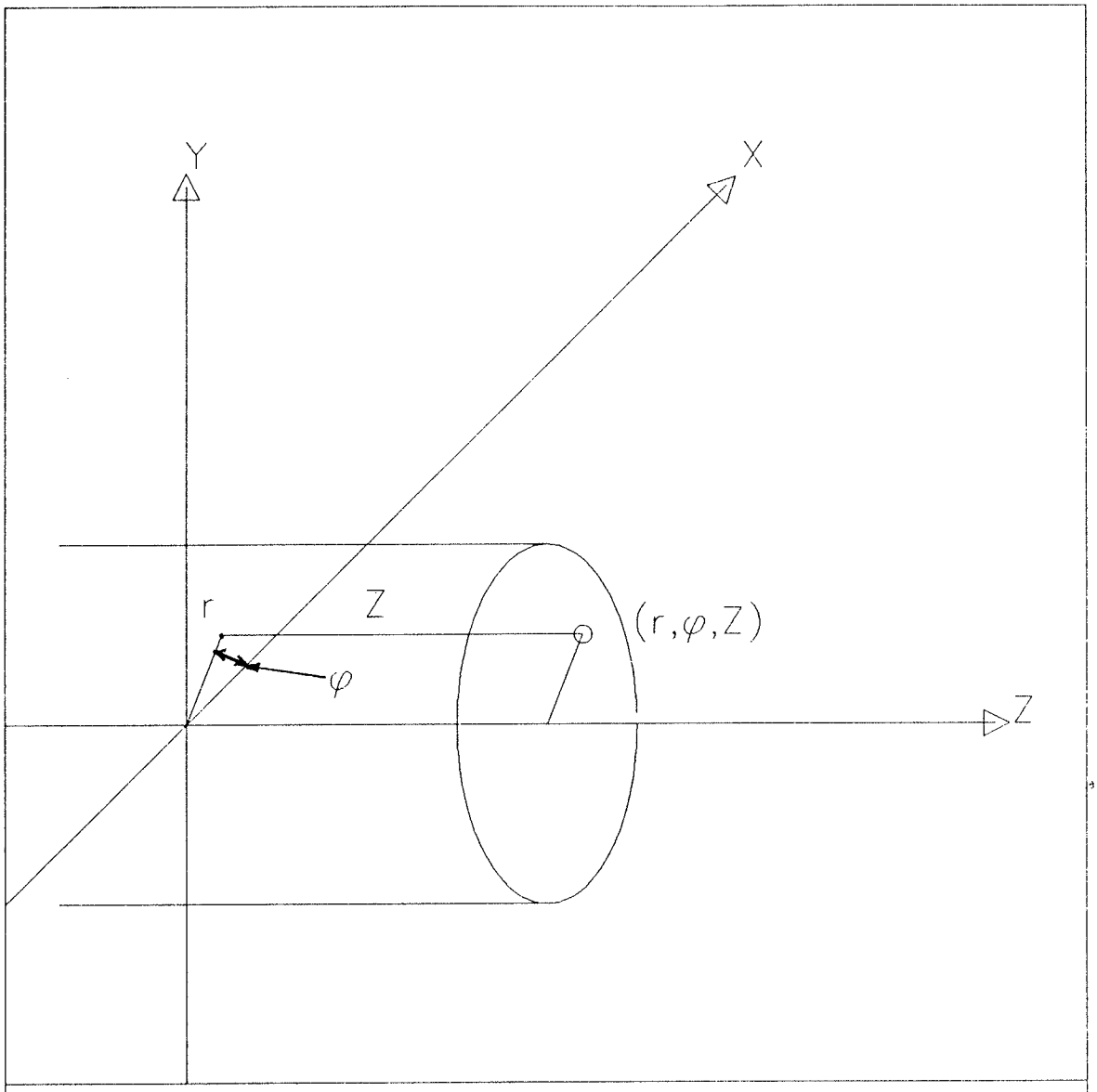

Fig. 3.1 :
Circular Waveguide Represented
in Cylindrical Coordinate System

where

$$\psi_n^e = a_n \cos(n\phi)\, J_n[(k^2 - k_z^2)^{1/2} r]\, e^{jk_z z} \tag{3.2.11}$$

$$\psi_n^m = b_n \sin(n\phi)\, J_n[(k^2 - k_z^2)^{1/2} r]\, e^{jk_z z} \tag{3.2.12}$$

and $J_n(x)$ is the Bessel function of the first kind of order n and argument x.

Substituting Eqs. (3.2.11) and (3.2.12) into (3.2.9) and (3.2.10) and simplifying the result yields the transcendental equation

$$[u_{np}^2 J_n(u_{np}) + j\, \eta_z\, ka\, u_{np} J_n'(u_{np})][u_{np}^2 J_n(u_{np}) + \frac{j}{\eta_\phi} ka\, u_{np} J_n'(u_{np})]$$

$$+ \frac{\eta_z}{\eta_\phi} n^2 (k^2 a^2 - u_{np}^2) J_n^2(u_{np}) = 0 \tag{3.2.13}$$

where the prime denotes differentiation with respect to the argument. The order of the zeros of this transcendental equation are given by the subscript p and

$$u_{np} = (k^2 - k_z^2)^{1/2} a. \tag{3.2.14}$$

When $\eta_\phi = \eta_z = \eta$ corresponding to an isotropic wall impedance condition, Eq. (3.2.13) leads to

$$[u_{np}^2 J_n(u_{np}) + j\, \eta\, ka\, u_{np} J_n'(u_{np})][u_{np}^2 J_n(u_{np}) + \frac{j}{\eta} ka\, u\, J_n'(u_{np})]$$

$$+ n^2 (k^2 a^2 - u_{np}^2) J_n^2(u_{np}) = 0 \tag{3.2.15}$$

which is identical to Eq. 1 in a paper by Mohsen and Hamid [1970].

By setting $\eta_\phi = \eta_z = 0$, the case for perfectly conducting walls, Eq. (3.2.13) becomes

$$[u_{np}^2 J_n(u_{np})]\, [jka u_{np} J_{np}'(u_{np})] = 0 \tag{3.2.16}$$

therefore;

$$J_n(u_{np}) = 0 \quad or \quad J_n'(u_{np}) = 0 \tag{3.2.17}$$

which are the characteristic equations for the TE and TM modes in a circular cylindrical waveguide with a perfectly conducting wall.

For large ka and imperfectly conducting walls, Eq. (3.2.13) reduces to

$$n\ J_n(u_{np}) \pm u_{np}\ J_n'(u_{np}) = 0 \tag{3.2.18}$$

provided neither η_ϕ nor η_z is zero. Eqs. (3.2.18) are the characteristic equations for balanced HE and EH modes in a circular cylindrical waveguide [Clarricoats and Olver 1984].

For $\eta_z = \infty$ and $\eta_\phi = 0$, which corresponds to a corrugated waveguide with one-quarter wavelength slots, Substitution into Eq. (3.2.13) yields;

$$nJ_n(u_{np}) \pm \frac{k}{k_z} u_{np}\ J_n'(u_{np}) = 0 \tag{3.2.19}$$

which are the characteristic equations for the unbalanced hybrid modes in a circular cylindrical waveguide.

3.3 RESULTS

Equation (3.2.13) shows explicitly how the eigenvalues (u_{np}) of the propagating modes are dependent on the mode number, ka, frequency and wall impedance. Furthermore, it is evident that for imaginary wall impedances with k greater than k_z the resulting eigenvalues are real. However, for complex or real values of wall impedance the resulting eigenvalues and propagation constant k_z are complex, signifying attenuation of a $\hat{z}$ directed wave. This is expected since a real surface impedance corresponds to lossy walls which would obviously attenuate the waves. The eigenvalues are determined numerically using the ZXSSQ

minimization routine (IMSL [1984]). The sum of the squares of the real and imaginary parts of the transcendental equation is minimized using a finite difference Levenberg-Marquardt algorithm and the resulting eigenvalues are accurate up to at least 5 decimal points.

In the paper by Mohsen and Hamid [1970] only real values of the relative surface impedance are considered, leading to complex eigenvalues which are incorrect. Corrections have been made to table 1 in Mohsen and Hamid [1970] and are presented in table 3.1 for $ka = 10$ and $\eta_z = \eta_\phi = 1$. In tables 3.2 and 3.3 values of u_{np} are also shown fo $\eta_\phi = \eta_z = 1$ and $ka = 5$ and 20, respectively. Table 3.4 lists the eigenvalues of the characteristic equation for a cylindrical waveguide with a lossless wall impedance for $ka = 10$, $\eta_z = j2.5$ and $\eta_\phi = j0.4$. As expected from the earlier analysis, all of the eigenvalues are real in this case. Although these eigenvalues are for hybrid modes, these modes are not neccessarily balanced hybrid modes, and are useful in designing feeds for center-fed parabolic reflector antennas.

Figure 3.2 diplays the graph of the eigenvalue of the fundamental mode (HE_{11}) vs. ka based on Eq. (3.2.13) for various values of wall impedance. In all of these cases the wall impedances in the two tangential directions are related by the expression $\eta_\phi \eta_z = -1$. It was found that if $\eta_\phi = j0.41583$ and $\eta_z = j2.40483$ then $u_{11} = 2.40483$ for all values of ka above cutoff ($ka = 1.3569$), which is the smallest allowable value of ka for the TE_{11} mode to propagate in a perfectly conducting waveguide). This eigenvalue signifies the balanced HE_{11} mode and shows that balanced hybrid conditions can be established in cylindrical waveguides with a small ka without using corrugations.

Figure 3.3 presents the asymptotic behavior of the eigenvalue of the HE_{11} mode as ka increases for real wall impedance, evaluated using Eq. (3.2.15). As can be seen from the figure, the real part of the eigenvalue approaches 2.4048

p	n					
	0	1	2	3	4	5
1	3.765 - j 0.389	2.379 - j 0.243	3.805 - j 0.405	5.122 - j 0.573	6.393 - j 0.765	7.637 - j 1.004
2	6.816 - j 0.792	5.009 - j 0.525	6.169 - j 0.651	8.239 - j 1.152	8.301 - j 0.862	9.273 - j 0.917
3	9.517 - j 1.201	5.431 - j 0.606	9.565 - j 1.343	10.182 - j 1.040	9.365 - j 1.475	12.428 - j 0.732
4	12.067 - j 1.076	8.047 - j 0.951	11.823 - j 0.955	13.339 - j 1.192	11.254 - j 0.891	12.968 - j 1.447
5	15.018 - j 0.790	8.316 - j 1.087	12.058 - j 1.253	16.332 - j 0.873	14.425 - j 0.645	15.904 - j 1.078
6	18.110 - j 0.618	10.635 - j 1.146	14.933 - j 0.925	19.457 - j 0.674	14.624 - j 1.131	19.057 - j 0.798
7	21.233 - j 0.510	10.793 - j 1.284	18.016 - j 0.704	22.608 - j 0.550	17.640 - j 0.516	22.255 - j 0.629
8	24.365 - j 0.436	13.446 - j 0.858	21.145 - j 0.568	13.111 - j 0.774	20.868 - j 0.650	25.451 - j 0.520

Table 3.1

u_{np} for $ka = 10$ and $\eta_\phi = \eta_z = 1.0$.

p	n					
	0	1	2	3	4	5
1	3.487 - j 0.731	2.277 - j 0.490	3.573 - j 0.895	6.494 - j 0.631	5.458 - j 1.541	8.797 - j 0.399
2	5.930 - j 0.943	4.508 - j 0.851	5.450 - j 0.807	9.788 - j 0.424	7.637 - j 0.490	9.263 - j 1.139
3	8.740 - j 0.635	4.798 - j 1.044	8.472 - j 0.533	9.907 - j 0.783	8.150 - j 1.155	12.348 - j 0.303
4	11.820 - j 0.449	7.154 - j 0.710	8.605 - j 0.831	13.027 - j 0.327	11.183 - j 0.743	12.439 - j 0.711
5	14.944 - j 0.347	7.278 - j 0.891	11.670 - j 0.551	13.057 - j 0.524	14.380 - j 0.282	15.732 - j 0.485
6	18.078 - j 0.284	10.237 - j 0.586	14.816 - j 0.406	16.241 - j 0.391	14.408 - j 0.503	18.994 - j 0.367
7	21.216 - j 0.240	13.347 - j 0.425	17.970 - j 0.322	19.418 - j 0.312	17.631 - j 0.378	22.225 - j 0.296
8	24.355 - j 0.208	16.482 - j 0.333	21.123 - j 0.267	22.588 - j 0.260	20.835 - j 0.303	28.629 - j 0.214

Table 3.2

u_{np} for $ka = 5$ and $\eta_\phi = \eta_z = 1.0$.

p	n					
	0	1	2	3	4	5
1	3.817 - j 0.193	2.399 - j 0.121	3.827 - j 0.194	5.135 - j 0.263	6.388 - j 0.331	7.608 - j 0.400
2	6.985 - j 0.363	5.505 - j 0.283	6.337 - j 0.323	7.526 - j 0.385	8.685 - j 0.447	9.821 - j 0.508
3	10.120 - j 0.554	8.366 - j 0.441	7.004 - j 0.367	10.955 - j 0.594	9.770 - j 0.535	11.092 - j 0.624
4	13.226 - j 0.786	8.625 - j 0.461	10.150 - j 0.561	11.607 - j 0.666	12.188 - j 0.670	14.397 - j 0.909
5	16.262 - j 1.093	11.738 - j 0.672	12.883 - j 0.741	14.181 - j 0.836	13.018 - j 0.780	16.636 - j 1.024
6	19.049 - j 1.445	14.635 - j 0.903	13.273 - j 0.800	17.751 - j 1.367	16.178 - j 1.127	17.548 - j 1.357
7	21.615 - j 1.409	14.820 - j 0.943	15.972 - j 1.023	19.978 - j 1.356	18.428 - j 1.231	19.542 - j 1.265
8	24.498 - j 1.118	17.600 - j 1.237	16.332 - j 1.133	20.328 - j 1.660	19.026 - j 1.618	22.375 - j 1.066

Table 3.3

u_{np} for $ka = 20$ and $\eta_\phi = \eta_z = 1.0$.

p	n					
	0	1	2	3	4	5
1	3.993	2.404	3.815	5.092	6.295	7.444
2	6.756	5.067	6.344	7.586	8.814	10.040
3	7.305	8.214	7.079	10.927	9.751	10.996
4	9.806	12.167	9.591	11.801	12.238	13.536
5	12.857	14.352	12.710	14.092	15.448	16.784
6	13.838	15.424	13.676	15.126	18.595	17.891
7	15.913	17.418	15.799	18.419	19.850	19.959
8	20.308	20.489	18.882	20.314	21.720	21.246
9	22.047	21.893	20.197	21.684	23.136	24.556

Table 3.4

u_{np} for $ka = 10$ and $\eta_z = j\ 2.5$ and $\eta_\phi = j\ 0.4$.

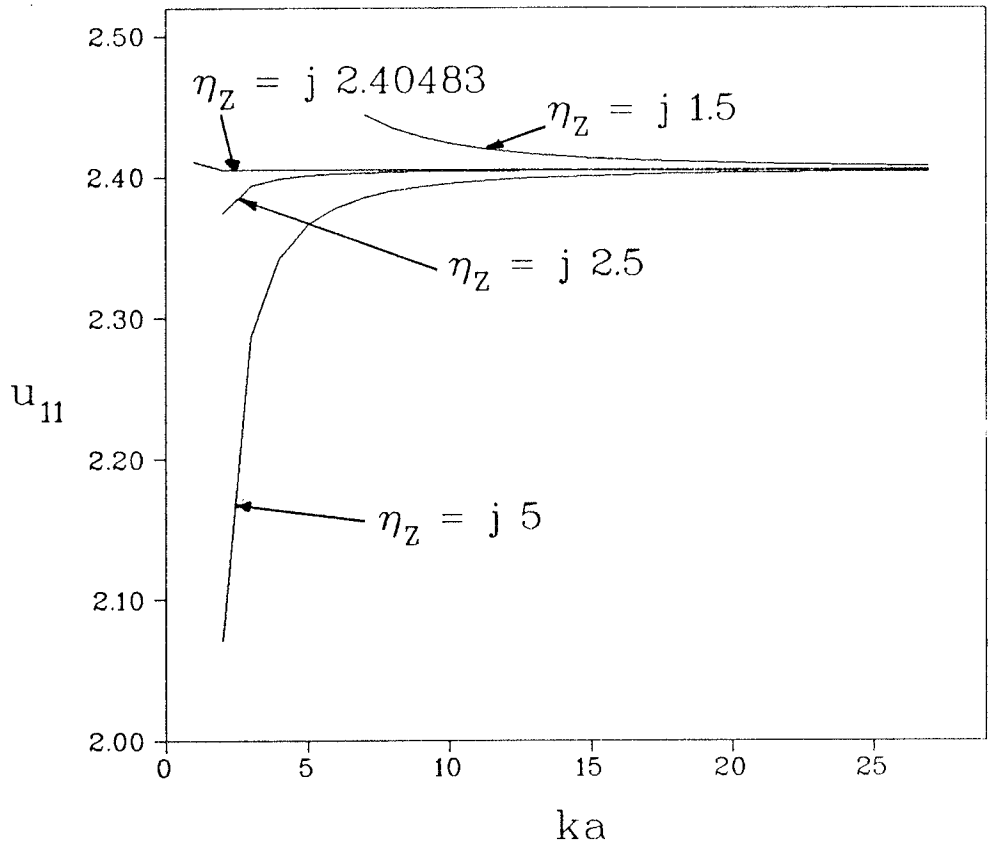

Fig. 3.2 : u_{11} vs. ka for various values of η_Z.

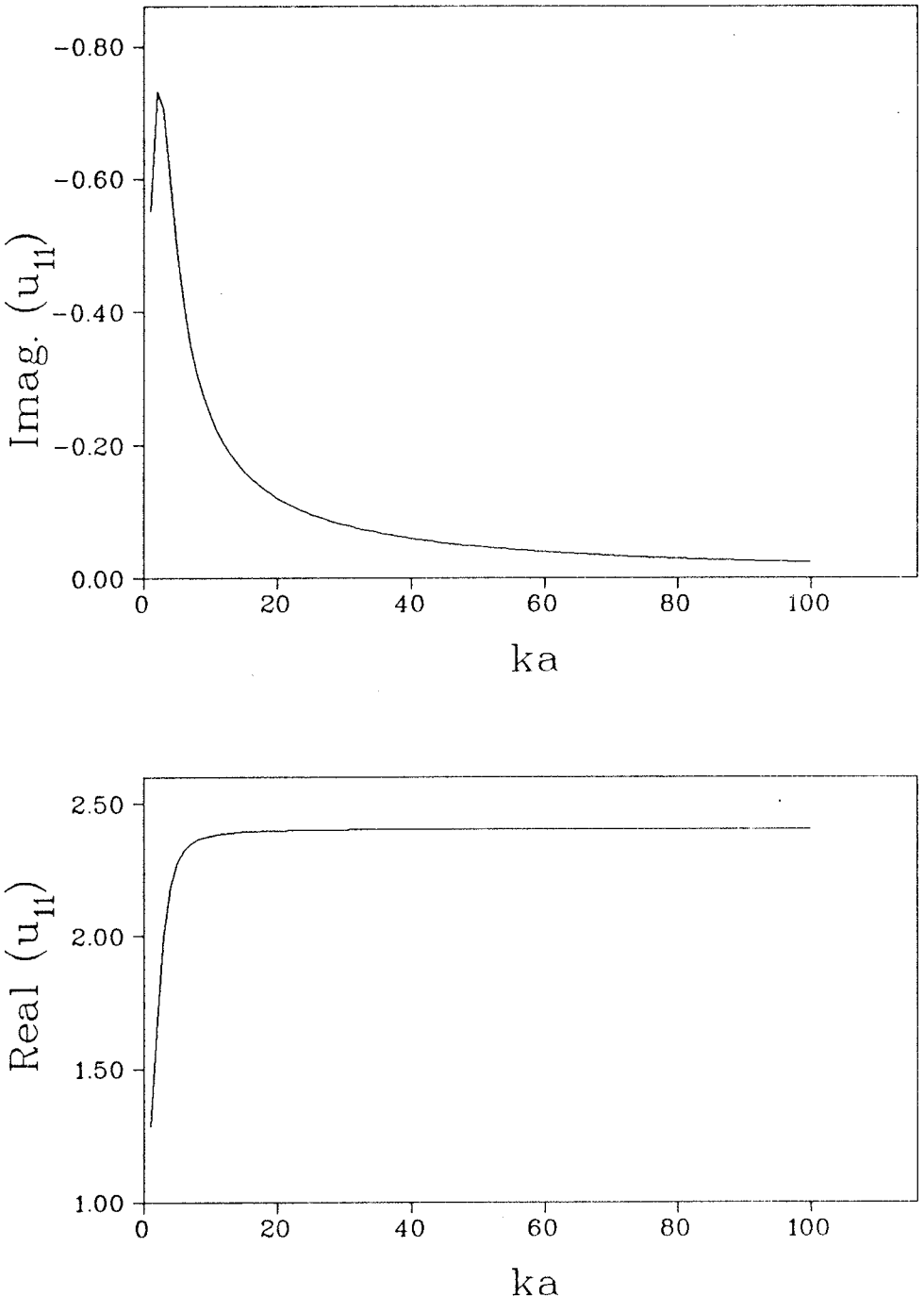

Fig. 3.3 : Real and Imaginary parts of u_{11} vs. ka for η = 1.0.

which is the eigenvalue of the balanced HE_{11} mode. At the same time, the imaginary part of the eigenvalue approaches zero. This result is supported in a paper by Dragone [1981] which predicts the propagation of hybrid modes for waveguides with impedance walls and only for large ka. This result is also verified by Eq. (3.2.18) which shows that for large values of ka the balanced hybrid mode propagates for any non-zero value of wall impedance. The one exception to this is if both tangential impedances are equal and approach infinity. This case is shown in Fig. 3.4 where it can be seen that the eigenvalue of the fundamental mode approaches the TE_{11} eigenvalue for large η and for several values of ka. Fig. 3.5 displays the corresponding behavior of the propagation constant for the same values of ka as in Fig. 3.4 as a function of the isotropic wall impedance η.

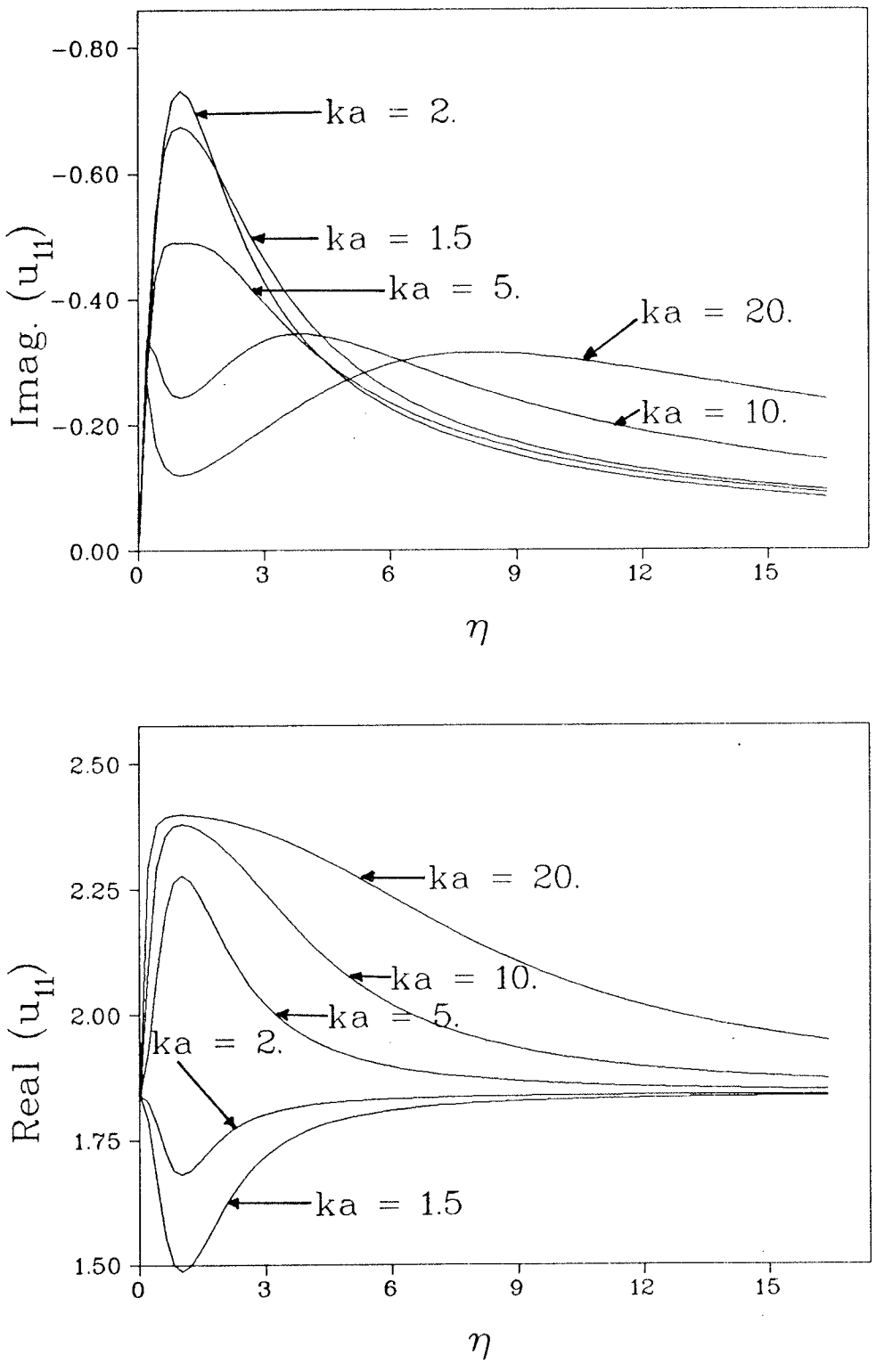

Fig. 3.4 : Real and Imaginary parts of u_{11} vs. η.

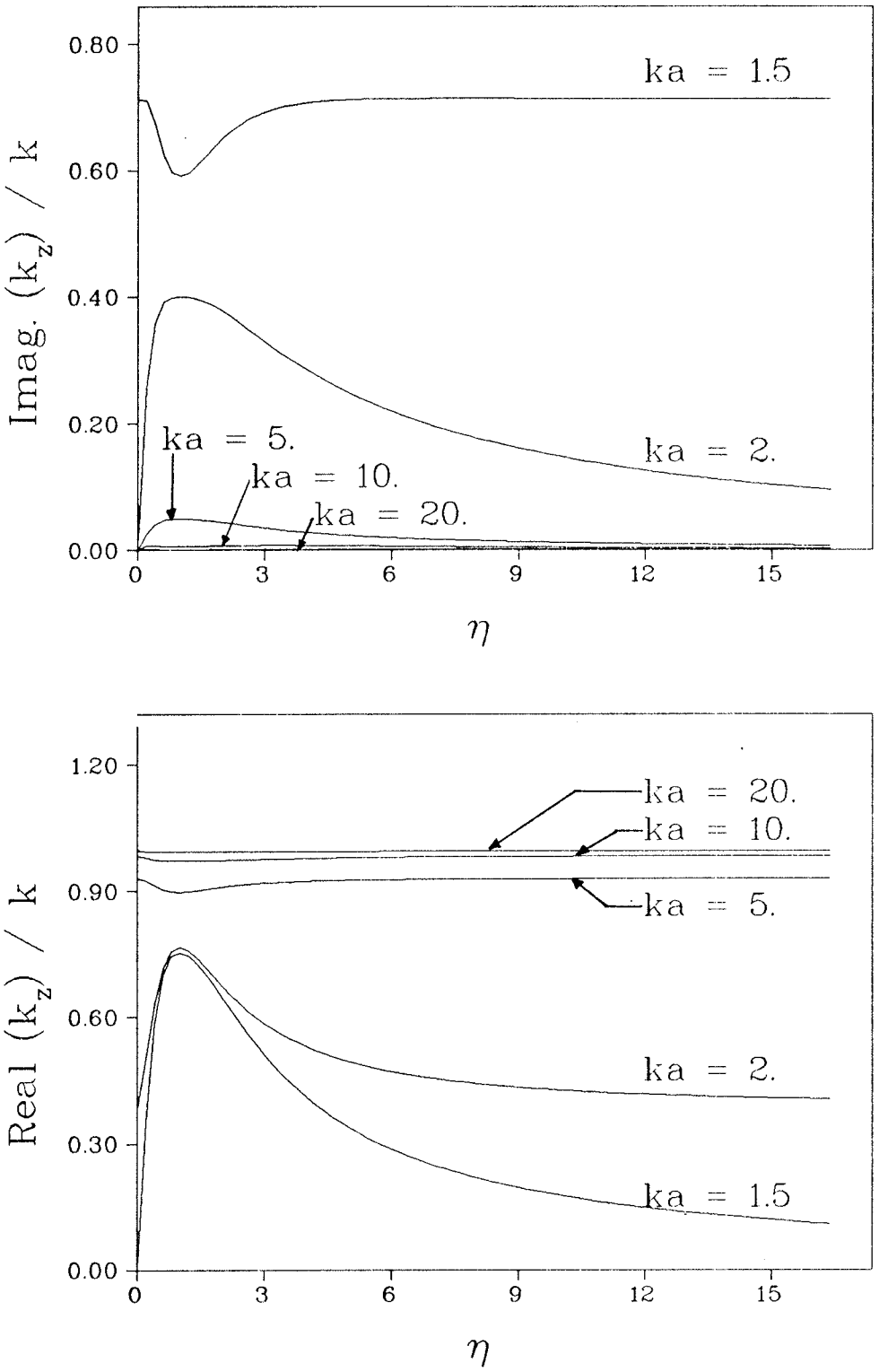

Fig. 3.5 : Real and Imaginary parts of k_z vs. η for n = p = 1.

Chapter 4 : THE BOUNDARY VALUE PROBLEM FOR CONICAL STRUCTURES

One method of investigating the propagation of electromagnetic energy in conical horns is to solve the corresponding problem in a conical waveguide. Since a conical waveguide can be simply described by a spherical coordinate system, it is possible to solve the wave equation by a separation of variables technique. The solution becomes a summation of spherical modes whose eigenvalues depend on the boundary conditions at the wall.

For a conical waveguide with perfectly conducting walls, the tangential E-field at the walls must be zero. This produces TE and TM modes analogous to the cylindrical waveguide case [Schorr and Beck 1950]. An azimuthally corrugated conical waveguide can support hybrid modes since the tangential E-field in the radial direction at the boundary no longer has to vanish, while the azimuthal components of the electric and magnetic fields vanish simultaneously.

A third situation arises when a dielectric is placed inside the horn. One such structure consists of a solid dielectric insert held away from the wall by another shell of dielectric of a lower permittivity. [Lier 1986]. This structure will support hybrid modes as long as the innermost dielectric cone is of a higher permittivity.

This thesis presents yet another conical structure which can support hybrid modes. This new structure consists of a dielectric lining on the walls of a conical horn. It is found that in order to support hybrid modes it is necessary to taper the surface impedance of the dielectric-air interface.

If the dielectric is not tapered, the transverse eigenvalue method cannot be applied and it is necessary to resort to the radial eigenvalue method [Hadidi 1985]. The transverse method fails even for a tapered dielectric insert since the eigenvalues become a function of the radial distance except for a special case which will be discussed later.

4.1 Solution of the Wave Equation

The Helmholtz wave equation in spherical coordinates is given by,

$$\frac{1}{R^2}\frac{d}{dR}\left(R^2\frac{d\phi}{dR}\right)+\frac{1}{R^2\sin\theta}\frac{d}{d\theta}\left(\sin\theta\frac{d\psi}{d\theta}\right)+\frac{1}{R^2\sin^2\theta}\frac{d^2\psi}{d\phi^2}+k^2\psi=0 \quad (4.1.1)$$

where the coordinate system used is shown in Fig. 4.1.

Letting

$$\psi=G(R)\,H(\theta)\,P(\phi). \quad (4.1.2)$$

Now, dividing Eq. (4.1.1) by (4.1.2) and multplying through by $R^2\sin^2\theta$ we obtain;

$$\frac{\sin^2\theta}{G}\frac{d}{dR}\left(R^2\frac{dG}{dR}\right)+\frac{\sin\theta}{H}\frac{d}{d\theta}\left(\sin\theta\frac{dH}{d\theta}\right)+\frac{1}{\Phi}\frac{d^2\Phi}{d\phi^2}+k^2R^2\sin^2\theta=0 \quad (4.1.3)$$

By setting $\frac{1}{\Phi}\frac{d^2\Phi}{d\phi^2}=-m^2$ and substituting into Eq. (4.1.3) and dividing by $\sin^2\theta$ we obtain;

$$\frac{1}{G}\frac{d}{dR}\left(R^2\frac{dG}{dR}\right)+\frac{1}{H\sin\theta}\frac{d}{d\theta}\left(\sin\theta\frac{dH}{d\theta}\right)-\frac{m^2}{\sin^2\theta}+k^2R^2=0. \quad (4.1.4)$$

Now the R and ϕ dependence has been separated. Choosing

$$\frac{1}{H\sin\theta}\frac{d}{d\theta}\left(\sin\theta\frac{dH}{d\theta}\right)-\frac{m^2}{\sin^2\theta}=-n(n-1) \quad (4.1.5)$$

and substituting this into Eq. (4.1.4) we obtain;

$$\frac{1}{G}\frac{d}{dR}\left(R^2\frac{dG}{dR}\right)-n(n+1)+k^2R^2=0.$$

Eq. (4.1.1) is now separated into three equations, each dependent on a single variable. The three equations are;

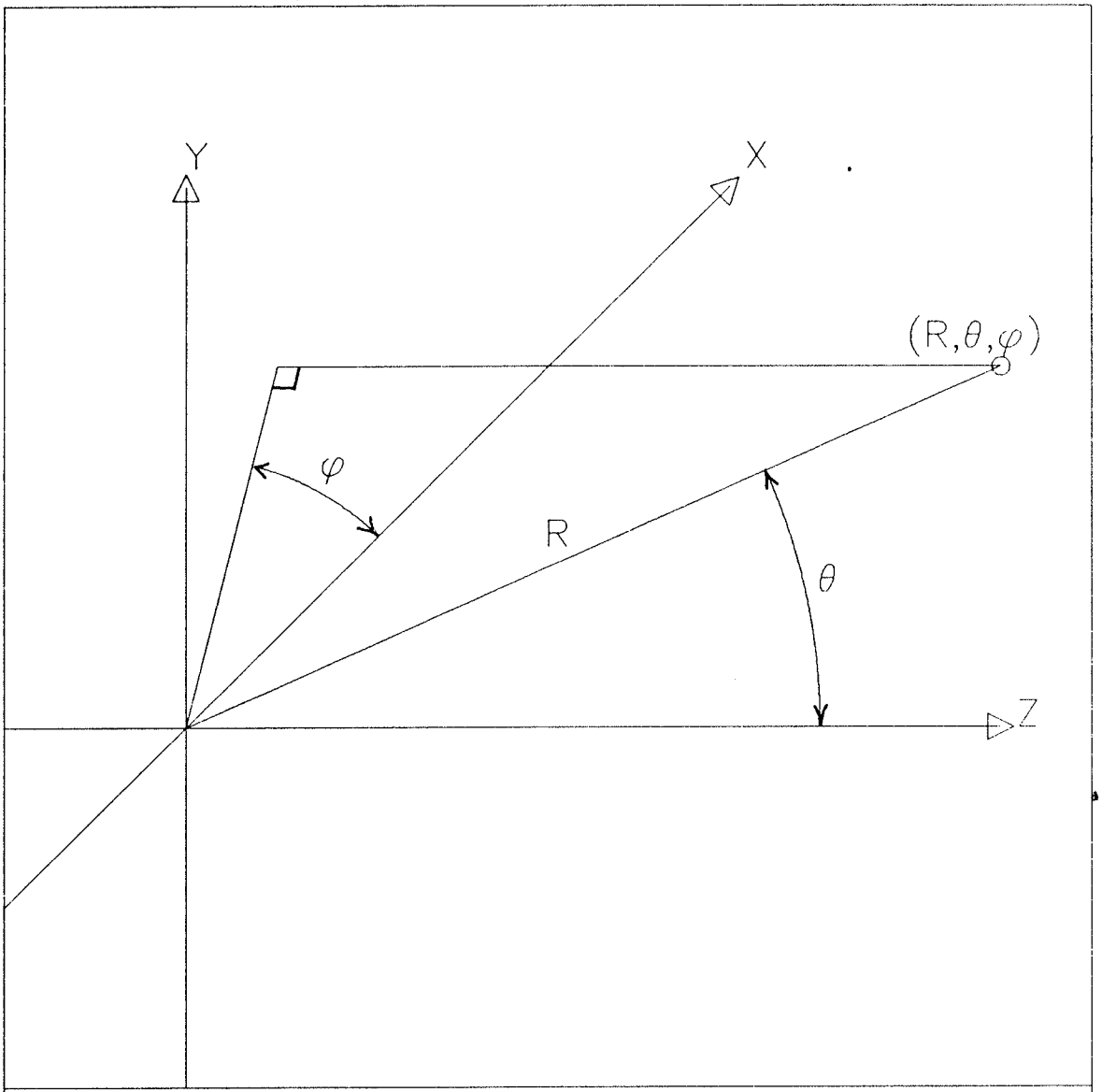

Fig. 4.1 :
Spherical Coordinate System

$$\frac{d}{dR}\left[R^2\frac{dG}{dR}\right]+\left[(kR)^2-n(n+1)\right]=0 \tag{4.1.6a}$$

$$\frac{1}{\sin\theta}\frac{d}{d\theta}\left[\sin\theta\frac{dH}{d\theta}\right]\left[n(n+1)-\frac{m^2}{\sin^2\theta}\right]=0 \tag{4.1.6b}$$

$$\frac{d^2\Phi}{d\phi^2}+m^2\Phi=0. \tag{4.1.6c}$$

The solution to equation (4.1.6c) is;

$$\Phi=a_1e^{(-jm\phi)}+a_2e^{(jm\phi)},$$

while the solution to Eq. (4.1.6b) is the associated Legendre function which can be written as;

$$H(\theta)=P_v^m(cos(\theta)).$$

An alternative method for solving Eq. (4.1.6b) is to make an approximation for small θ. By making the approximation $\sin\theta=\theta$ Eq. (4.1.6b) is reduced to the Bessel equation [Narasimhan 1973]. The asymptotic solution is given as ;

$$H(\theta)=J_m(q\theta)$$

where $q=(s(s+1))^{1/2}$ and $s=-.5+(.25+(\frac{p_{mn}}{\alpha_0})^2)^{1/2}$. In this case, p_{mn} is dependent on the type of waveguide being investigated but in general it can be found from the roots of a function involving the Bessel function and/or its derivatives. This approximation is extremely useful for numerical work or for applying analytic solutions to practical problems, due mainly to the difficulties involved in calculating the associated Legendre function. Although the approximation is only valid for small values of θ it has been found to be useful even for wide flare angles [Narasimhan 1973].

The solution to Eq. (4.1.6a) is the spherical Hankel function. In most cases involving conical horns the Hankel function of the second kind is used since this represents an outward travelling wave if the $e^{j\omega t}$ time convention is used. Although the Hankel function becomes infinite at $R=0$, this is not a problem in practical horn design for two reasons. Firstly, a horn is usually fed by a cylindrical waveguide at the apex end. In this case, the horn never does reach a point where $R=0$. Secondly, the region at the apex of conical waveguide is very highly attenuating and no power ever reaches the apex (Schorr and Beck 1950). Thus, the solutions to Eq. (4.1.6a) can be written as;

$$G=H_n(kR).$$

This spherical Hankel function can be written in terms of the cylindrical Hankel function as;

$$h_n(kR)=\sqrt{\frac{\pi}{2kR}}H_{n+\frac{1}{2}}(kR).$$

Thus the complete solution to the wave equation in a conical region may be written as;

$$\psi=P_\nu^m(\cos\theta)h_n(kR)e^{jm\phi} \quad (exact) \tag{4.1.7}$$

$$\psi=J_m(q\theta)h_n(kR)e^{jm\phi} \quad (approximate). \tag{4.1.8}$$

Scalar electric and magnetic potentials can be written as;

$$A_R=\psi \quad , \quad F_R=\psi$$

The vector potentials can be written as;

$$\bar{A}=\hat{a}_R A_R \quad , \quad \bar{F}=\hat{a}_R A_R$$

However, the scalar potentials are not solutions of the scalar Helmholtz equation since $\nabla^2 A_R \neq (\nabla^2 \bar{A})_R$. The solution to the scalar Helmholtz equation is, in fact; $\frac{A_R}{R}$ and $\frac{F_R}{R}$. The Vecter potentials can therefore be written as;

$$\bar{A} = R\psi^a \hat{a}_R \quad , \quad \bar{F} = R\psi^f \hat{a}_R.$$

The fields in the horn can now be found from the following expressions;

$$\bar{E} = -\nabla \times R\psi^f + \frac{1}{\hat{y}} \nabla \times \nabla \times R\psi^a \tag{4.1.9}$$

$$\bar{H} = \nabla \times R\psi^a + \frac{1}{\hat{z}} \nabla \times \nabla \times R\psi^f. \tag{4.1.10}$$

In the last equation the ψ's are all multiplied by R so we can use the spherical Hankel function defined by Schelkunoff[1943].

$$\hat{H}_n(kR) = kRh_n(kR).$$

Now, from Eqs. (4.1.9/10) we can write out the fields explicitly as;

$$E_R = \frac{1}{\hat{y}} \left(\frac{d^2}{dR^2} + k^2 \right) A_R \tag{4.1.11}$$

$$E_\theta = \frac{-1}{R \sin\theta} \frac{dF_R}{d\phi} + \frac{1}{\hat{y}R} \frac{d^2 A_R}{dR\, d\theta} \tag{4.1.12}$$

$$E_\phi = \frac{1}{R} \frac{dF_R}{d\theta} + \frac{1}{\hat{y}R \sin\theta} \frac{d^2 A_R}{dR\, d\phi} \tag{4.1.13}$$

$$H_R = \frac{1}{\hat{z}} \left(\frac{d^2}{dR^2} + k^2 \right) F_R \tag{4.1.14}$$

$$H_\theta = \frac{1}{R \sin\theta} \frac{dA_R}{d\phi} + \frac{1}{\hat{z}R} \frac{d^2 F_R}{dR\, d\theta} \tag{4.1.15}$$

$$H_{\phi}=\frac{-1}{R}\frac{dA_R}{d\theta}+\frac{1}{\hat{z}R\sin\theta}\frac{d^2F_R}{dRd\phi} \qquad (4.1.16)$$

where;

$$A_R \text{ or } F_R = P_{\nu}^{m}(\cos\theta)\,\hat{H}_n(kR)\,e^{jm\phi} \qquad (exact)$$

$$A_R \text{ or } F_R = J_m(q\theta)\,\hat{H}_n(kR)\,e^{jm\phi} \qquad (approximate).$$

4.2 A Perfectly Conducting Wall

Up to this point in the analysis there have been no boundary conditions applied to these solutions since they are valid for any region which can be described in the spherical coordinate system. In the case of a conical waveguide with a perfectly conducting wall the boundary conditions at the wall are;

$$E_\phi = 0 \text{ and } E_R = 0 \tag{4.2.1}$$

Both TE and TM modes can exist in conical waveguide so we may write;

$$F_R = 0 \text{ , } TM \text{ modes}$$

$$A_R = 0 \text{ , } TE \text{ modes.} \tag{4.2.2}$$

Applying the boundary conditions at the wall we obtain, for the exact formulation;

$$P_\nu^m(\cos\theta_1) = 0 \quad \text{for } TM \text{ modes}$$

$$\left(\frac{d}{d\theta} P_\nu^m(\cos\theta)\right)_{\theta=\theta_1} = 0 \quad \text{for } TE \text{ modes.} \tag{4.2.3}$$

The solution of these eigenfunctions will supply values for ν, the order of the Legendre function. Likewise, the boundary conditions may be applied to the approximate solution for the fields to yield;

$$J_m(q\theta_1) = 0 \quad \text{for } TM \text{ modes}$$

$$\left(\frac{d}{d\theta} J_m(q\theta)\right)_{\theta=\theta_1} = 0 \quad \text{for } TE \text{ modes.} \tag{4.2.4}$$

Although there are graphs in a report by Kay [1962], there is no complete set of tables available for the eigenvalues of Eq. (4.2.3), which is one of the reasons why

the approximate eigenfunctions given in Eq. (4.2.4) are very useful. In practice this approximate solution is much easier to work with and, although it is valid only for small flare angles, it has been shown to provide acceptable results for flare angles up to 60 degrees [Narisimhan 1973]. The field expressions for a conical waveguide are now completely known from Eqs. (4.1.11)-(4.1.16).

4.3 Corrugated Walls

As has been described in section 4.1, surface impedances have been used to model corrugated walls in several types of waveguides including circular cylindrical [Clarricoats and Olver 1984] and conical [Clarricoats and Saha 1971] waveguides. The analysis of the corrugated conical waveguide leads directly to spherical hybrid modes which are analogous to the hybrid modes developed in cylindrical waveguide.

Corrugated conical waveguides have been analyzed in the literature using two models. For horns with a narrow flare angle (less than approximately 30 degrees) the waveguide can be treated as a circular cylindrical waveguide with a varying diameter [Dragone 1980]. Horns with half-flare angles greater than 30 degrees must be analysed using spherical coordinates [Clarricoats and Olver 1984]. This section is concerned with the analysis using a spherical coordinate system.

The boundary conditions for a conical waveguide with corrugations in the ϕ direction are;

$$\frac{E_\phi}{H_R} = Z_1 = 0 \quad \text{and} \quad \frac{H_\phi}{E_R} = Y_1 \quad at \ \theta = \theta_1 \,. \tag{4.3.1}$$

In the above equation Z_1 is equal to zero since the E-field in the ϕ direction is shorted by the continuous ridge of metal in the ϕ direction. In the radial (R) direction the waveguide wall is discontinuous and the impedance is dependent on the depth, shape and width of the corrugations. Setting $Y_1 = 0$ gives rise to the spherical hybrid modes in corrugated waveguide. Fig. 4.2 shows the geometry of a corrugated horn.

Assuming an $e^{j\omega t}$ time dependence, the radial fields of a spherical mode in a conical waveguide can be written as;

$$E_R = \frac{A\nu(\nu+1)}{jkR^2} \hat{H}_\nu^2(kR)\, P_\nu^m(\cos\theta) \cos m\phi \tag{4.3.2}$$

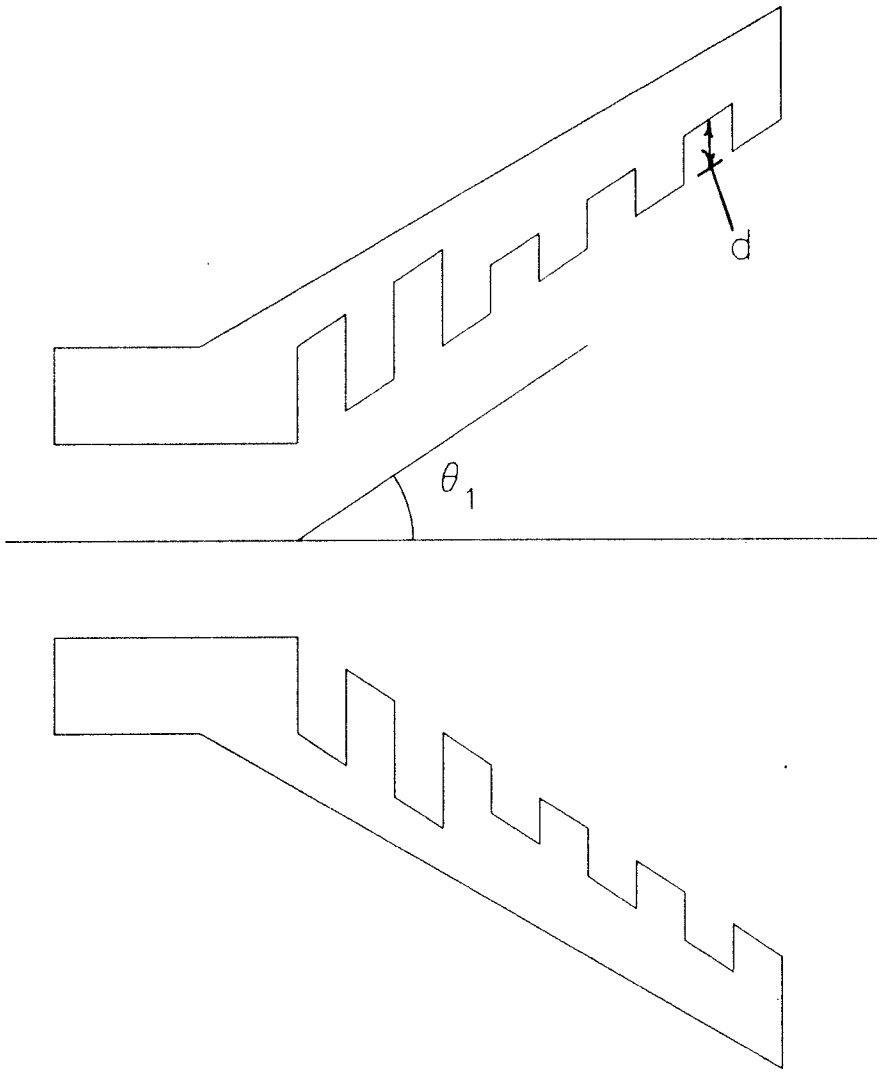

Fig. 4.2 :
Geometry of the
Corrugated Horn

$$Y_0 H_R = \frac{A\bar{\Lambda}\nu(\nu+1)}{jkR^2}\,\hat{H}_\nu^2(kR)\,P_\nu^m(\cos\theta)\sin m\phi \qquad (4.3.3)$$

where $P_\nu^m(\cos\theta)$ is the associated Legendre function of order m and degree ν ;

$\bar{H}_\nu^2(kR)$ is the spherical Hankel function of the second kind and order ν ;

Y_0 is the admittance of free space;

$\bar{\Lambda}$ is the hybrid factor possessing a characteristic frequency dependent value for each mode,

and the coordinate system used is shown in Fig. 4.1.

The transverse fields can be obtained from Eqs. (4.3.2) and (4.3.3) as;

$$RE_\theta = -A\bar{H}_\nu^2(kR)\left[\bar{\beta}P_\nu^{m\prime}(\cos\theta)+m\bar{\Lambda}\frac{P_\nu^m(\cos\theta)}{\sin\theta}\right]\cos m\phi \qquad (4.3.4)$$

$$RE_\phi = A\bar{H}_\nu^2(kR)\left[\bar{\Lambda}P_\nu^{m\prime}(\cos\theta)+m\bar{\beta}\frac{P_\nu^m(\cos\theta)}{\sin\theta}\right]\sin m\phi \qquad (4.3.5)$$

$$Y_0 RH_\theta = -A\bar{H}_\nu^2(kR)\left[\bar{\Lambda}\bar{\beta}P_\nu^{m\prime}(\cos\theta)+m\frac{P_\nu^m(\cos\theta)}{\sin\theta}\right]\sin m\phi \qquad (4.3.6)$$

$$Y_0 RH_\phi = -A\bar{H}_\nu^2(kR)\left[P_\nu^{m\prime}(\cos\theta)+m\bar{\Lambda}\bar{\beta}\frac{P_\nu^m(\cos\theta)}{\sin\theta}\right]\cos m\phi \qquad (4.3.7)$$

where $\bar{\beta}(R)=\dfrac{j\hat{H}_\nu^{2\prime}(kR)}{\hat{H}_\nu^2(kR)}$ and the prime indicates differentiation with respect to the arguement.

Up to this point in the analysis these equations are not dependent on which type of horn is being considered.

The tangential fields at the boundary of the waveguide may be written in terms of the boundary conditions as;

$$\frac{H_\phi}{E_r}=\frac{j\omega\epsilon_0 R}{\nu(\nu+1)}\left[\sin\theta\frac{P'}{P}+\frac{m}{\sin\theta}\frac{\hat{H}'}{\hat{H}}\bar{\Lambda}\right]=Y_1 \tag{4.3.8}$$

$$\frac{E_\phi}{H_r}=\frac{j\omega\mu_0 R}{\nu(\nu+1)}\left[-\sin\theta\frac{P'}{P}+\frac{m}{\sin\theta}\frac{\hat{H}'}{\hat{H}}\frac{1}{\bar{\Lambda}}\right]=0. \tag{4.3.9}$$

By matching the boundary conditions at $\theta=\theta_1$ we have;

$$p_\nu^m(\theta_1)=\frac{-m\bar{\beta}}{\bar{\Lambda}\sin\theta_1} \tag{4.3.10}$$

and,

$$p_\nu^m(\theta_1)=\bar{Y}\nu(\nu+1)=\frac{-m\bar{\Lambda}\bar{\beta}}{\sin\theta_1} \tag{4.3.11}$$

where;

$$p_\nu^m(\theta_1)=\frac{\dfrac{dP_\nu^m(\cos\theta)}{d\theta}}{P_\nu^m(\cos\theta)} \quad at\ \theta=\theta_1 \tag{4.3.12}$$

and;

$$\bar{Y}=\frac{-j\ Y_1\ \eta_0}{kR}\ . \tag{4.3.13}$$

The average slot admittance, Y_1, is given to a good approximation by;

$$Y_1=-j\ \frac{(cot\ kd\ +\ \dfrac{1}{2kR\ \sin\theta_1})}{\eta_0}$$

where d is the depth of the slot and there are at least 3 slots per wavelength. Multiplying Eqs. (4.3.8) and (4.3.9) yields;

$$p_\nu^m(\theta_1)\left[p_\nu^m(\theta_1)-\bar{Y}\nu(\nu+1)\right]=\frac{m^2\bar{\beta}^2}{\sin^2\theta_1}\ . \tag{4.3.14}$$

Subtracting Eq. (4.3.8) from (4.3.9) yields;

$$\overline{\Lambda}-\frac{1}{\overline{\Lambda}}=\frac{\overline{Y}\,\nu(\nu+1)\sin\theta_1}{m\,\overline{\beta}} \tag{4.3.15}$$

Eq. (4.3.14) is the modal equation for ν and Eq. (4.3.15) gives the hybrid factor $\overline{\Lambda}$ in terms of the normalized wall admittance, $\overline{Y}$.

Eq. (4.3.14) is inconsistent with the separation-of-variables assumption made in section 4.1 unless the normalized admittance, $\overline{Y}$, is independent of R. This inconsistency can be avoided by choosing $kd=\frac{\pi}{2}$, thus setting $\overline{Y}=0$. For $m=1$ (lowest order mode) we may write equation (4.3.14) as;

$$f_{\nu}^{1}(\cos\theta_1)=\pm 1 \tag{4.3.16}$$

for the balanced case, where

$$f_{\nu}^{1}(\cos\theta_1)=p_{\nu}^{m}(\theta_1)\sin\theta_1 .$$

Also, from Eqs. (4.3.15)

$$\overline{\Lambda}=\pm j \tag{4.3.17}$$

The solutions of the two previous equations corresponding to the negative sign are termed the HE modes whereas the solutions corresponding to the positive sign are termed the EH modes. Of the two types of modes, the HE modes are more useful since they have a maximum on axis. The balanced HE_{11} mode is similar to a linear combination of the TE_{11} and the TM_{11} modes found in smooth conical waveguides since it provides a nearly linearly polarized aperture field.

The Legendre functions used to describe the hybrid-mode fields inside a conical structure can be approximated by making use of the following relations;

$$P_{\nu}^{1}(\cos\theta)=J_1(q\,\theta) \tag{4.3.18}$$

$$P_\nu^{1\prime}(\cos\theta)=q[J_1'(q\theta)] \tag{4.3.19}$$

where;

$$q = \sqrt{\nu(\nu+1)}\,.$$

The approximation to the field expressions can then be written as;

$$RE_\theta=-A\bar{H}_\nu^2(kR)q\left[\bar{\beta}J_1'(q\theta)+\bar{\Lambda}\frac{J_1(q\theta)}{q\theta}\right]\cos\phi \tag{4.3.20}$$

$$RE_\phi=A\bar{H}_\nu^2(kR)q\left[\bar{\Lambda}J_1'(q\theta)+\frac{\bar{\beta}J_1(q\theta)}{q\theta}\right]\sin\phi \tag{4.3.21}$$

$$Y_0RH_\theta=-A\bar{H}_\nu^2(kR)q\left[\bar{\beta}\bar{\Lambda}J_1'(q\theta)+\frac{J_1(q\theta)}{q\theta}\right]\sin\phi \tag{4.3.22}$$

$$Y_0RH_\phi=-A\bar{H}_\nu^2(kR)q\left[J_1'(q\theta)+\frac{\bar{\beta}\bar{\Lambda}J_1(q\theta)}{q\theta}\right]\cos\phi \tag{4.3.23}$$

where $\bar{\Lambda}>0$ signifies HE modes and $\bar{\Lambda}<0$ signifies EH modes.

Under balanced conditions, ($\bar{\Lambda}=\pm 1$), Eqs. (4.3.11) and (4.3.12) can be further simplified. Using the Bessel recurrence relations;

$$J_1'(x)=\tfrac{1}{2}[J_0(x)-J_2(x)]$$

$$\frac{J_1(x)}{x}=\tfrac{1}{2}[J_0(x)+J_2(x)]$$

and dropping the radial dependence, the field expressions may be written as;

$$E_\theta=-q[J_0(q\theta)]\cos\phi \tag{4.3.24}$$

$$E_\phi=+q[J_0(q\theta)]\sin\phi \tag{4.3.25}$$

$$H_\theta=+q[J_2(q\theta)]\cos\phi \tag{4.3.26}$$

$$H_{\phi}=+q\,[J_2(q\,\theta)]\sin\phi\ . \tag{4.3.27}$$

Using Eqs. (4.3.18) and (4.3.19), the characteristic equation (Eq. (4.3.16)) may be written as;

$$(1-\gamma)\,\frac{J_1(x)}{x}=J_0(x) \tag{4.3.28}$$

where $\gamma < 0$ for EH_{1n} modes and $\gamma > 0$ for HE_{1n} modes. The eigenvalues of Eq. (4.3.28) are given in table 4.1 for the first five modes.

Table 4.1a : HE_{1n} Mode Eigenvalues					
	Mode Number				
γ	1	2	3	4	5
0.00	1.8412	5.3314	8.5363	11.7060	14.8636
0.20	1.9844	5.3702	8.5600	11.7232	14.8771
0.40	2.1092	5.4085	8.5836	11.7404	14.8906
0.60	2.2192	5.4463	8.6072	11.7575	14.9041
0.80	2.3171	5.4835	8.6305	11.7745	14.9175
1.00	2.4048	5.5201	8.6537	11.7915	14.9309

Table 4.1b : EH_{1n} Mode Eigenvalues					
	Mode Number				
γ	1	2	3	4	5
-0.00	1.8412	5.3314	8.5363	11.7060	14.8636
-0.20	1.6741	5.2925	8.5126	11.6888	14.8501
-0.40	1.4739	5.2533	8.4887	11.6716	14.8366
-0.60	1.2235	5.2140	8.4649	11.6543	14.8230
-0.80	0.8797	5.1747	8.4411	11.6371	14.8095
-1.00	0.0000	5.1357	8.4173	11.6199	14.7960

4.4 A Dielectric Lined Wall

The following is an analysis of yet another conical structure which may support spherical hybrid modes. In this section the walls are handled simply as an impedance boundary and the conditions on this impedance are then found which will support hybrid modes. Figure 4.3 displays the general layout of the conical horn with surface impedances on the wall.

Following Clarricoats [1969], we have $\frac{E_\phi}{H_R}=Z_1$ and $\frac{H_\phi}{E_R}=Y_1$. From the field expressions in a conical region from section 4.1, if we set;

$$P'=\frac{dP_\nu^m(\cos\theta_1)}{d(\cos\theta_1)} \qquad \hat{H}'=\frac{d\hat{H}_\nu(kR)}{d(kR)}$$

$$P=P_\nu^m(\cos\theta_1) \qquad \hat{H}=\hat{H}_\nu(kR)$$

$$\gamma=j\frac{b_{mn}}{a_{mn}}\left(\frac{\epsilon_0}{\mu_0}\right)^{1/2}$$

then we may write;

$$\frac{H_\phi}{E_R}=j\omega\epsilon_0\frac{R}{\nu(\nu+1)}\left[\sin\theta_1\frac{P'}{P}+\frac{m}{\sin\theta_1}\frac{\hat{H}'}{\hat{H}}\gamma\right]=Y_1 \quad , \tag{4.4.1}$$

$$\frac{E_\phi}{H_R}=j\omega\mu_0\frac{R}{\nu(\nu+1)}\left[-\sin\theta_1\frac{P'}{P}+\frac{m}{\sin\theta_1}\frac{\hat{H}'}{\hat{H}}\frac{1}{\gamma}\right]=Z_1 \quad . \tag{4.4.2}$$

By solving for γ in Eq. (4.4.2) and substituting into Eq. (4.4.1), we can eliminate γ. Allowing R to become large so that $\left(\frac{\hat{H}'}{\hat{H}} \rightarrow -j\right)$ further simplifies Eqs. (4.4.1) and (4.4.2). After some manipulation we obtain:

$$\sin^2\theta_1\frac{P'}{P}\left(\sin^2\theta_1\frac{P'}{P}+\hat{c}\right)=m^2 \tag{4.4.3}$$

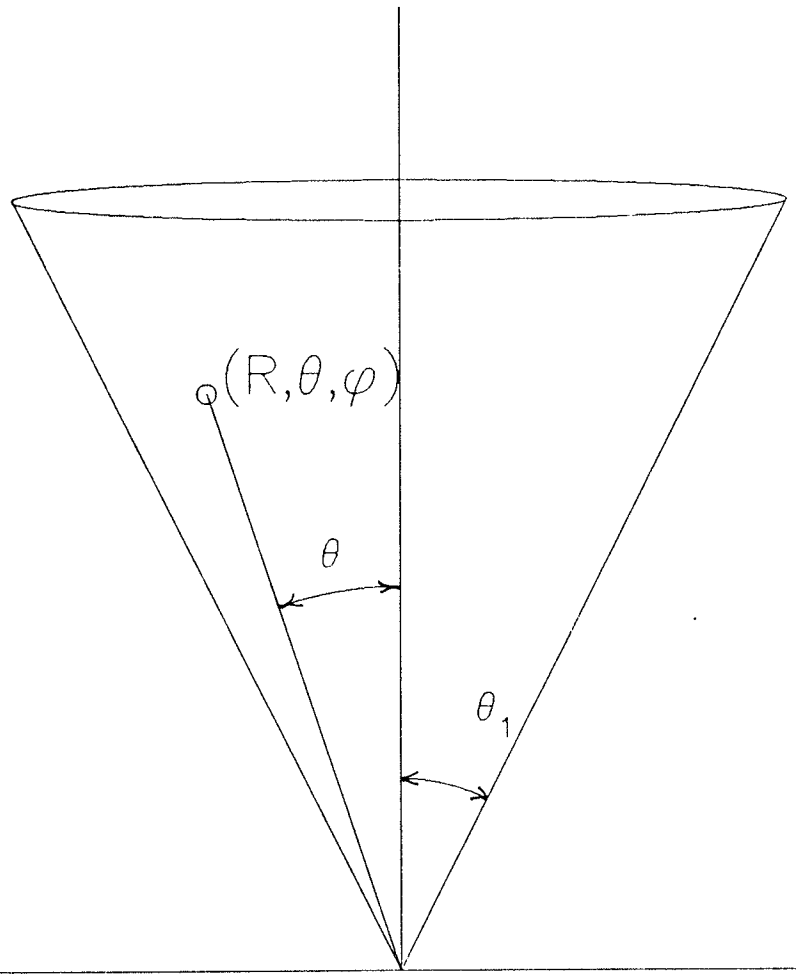

Fig. 4.3 :
Cone Represented in
Spherical Coordinate System

$$\hat{c}=PZ_1Y_1\frac{\nu^2(\nu+1)^2}{P'\epsilon_0\mu_0R^2\omega^2}-\frac{j\sin\theta_1\nu(\nu+1)(\epsilon_0Z_1-\mu_0Y_1)}{\omega\epsilon_0\mu_0R}\,. \tag{4.4.4}$$

In order for Eq. (4.4.3) to be consistent with the separation of variables assumption used to obtain the field expressions, it must be independent of R. In the analysis of hybrid modes in corrugated waveguide this inconsistency is avoided by setting $Y_1=0$. In the present analysis it can be avoided by setting $\hat{c}=0$.

Setting Eq. (4.4.4) to zero yields;

$$\frac{\mu_0Y_1-\epsilon_0Z_1}{Z_1Y_1}=j\left(\frac{P}{P'}\frac{\nu(\nu+1)}{\sin\theta_1\omega R}\right)\,. \tag{4.4.5}$$

Since both Y_1 and Z_1 are complex, another relation is needed in order to solve for them explicitly. There are, however, certain restrictions placed on Y_1 and Z_1 by Eq. (4.4.5). These restrictions are;

$$\mathrm{Re}\left(\frac{\mu_0Y_1-\epsilon_0Z_1}{Z_1Y_1}\right)=0 \tag{4.4.6}$$

$$\mathrm{Im}\left(\frac{\mu_0Y_1-\epsilon_0Z_1}{Z_1Y_1}\right)=\frac{P}{P'}\frac{\nu(\nu+1)}{\sin\theta_1\omega R}\,. \tag{4.4.7}$$

This is as far as the analysis can proceed without further knowledge of the relationship between the angular and radial surface impedances at the wall of a dielectric lined conical waveguide.

One possible condition on these impedances is that they are equal in both directions. This condition corresponds to setting $Y_1=\frac{1}{-\eta\eta_0}$ and $Z_1=\eta\eta_0$. From this process we obtain a quadratic of the form:

$$\eta^2+\frac{P}{P'}\frac{\nu(\nu+1)}{\eta_0R}\frac{1}{j\omega\sin\theta_1\epsilon_0}\eta+1=0 \tag{4.4.8}$$

the solutions to which are:

$$\eta_{\pm} = -\frac{P}{P'}\frac{\nu(\nu+1)}{2\eta_0 R}\frac{1}{j\omega\sin\theta_1\epsilon_0} \pm \left(\frac{-P^2}{(P')^2}\frac{\nu^2(\nu+1)^2}{4\eta_0^2R^2}\frac{1}{\omega^2\sin^2\theta_1\epsilon_0{}^2} - 1\right)^{1/2} \quad (4.4.9)$$

The analysis of the modes now proceeds exactly as in the corrugated waveguide case. Substituting $\hat{c}=0$ into Eq. (4.4.3) we obtain the eigenfunction identical to the corrugated waveguide case, i.e.;

$$\sin^2\theta_1\frac{P'}{P} = \pm m \ . \quad (4.4.10)$$

Equation (4.4.10) has been solved in the HE_{11} case (m=1) for flare semi-angles ranging between 16^0 and 90^0 [Clarricoats 1969]. Table 4.2 tabulates the impedance taper necessary to support an HE_{11} mode in a conical waveguide with a flare semi- angle of 16^0, 45^0 and 90^0 over a three decade range of R at 6 GHz. Figure 4.4 is a plot of the data in Table 4.2 for practical values of R. Only the positive roots of Eq. (4.4.8) have been plotted.

Table 4.2 : Roots of quadratic equation (4.4.8)

	$\theta_1=16^0$		$\theta_1=45^0$		$\theta_1=90^0$	
R	η_+	η_-	η_+	η_-	η_+	η_-
.01	j102.9	-j.00971	j35.59	-j.02809	j15.82	-j.06319
.02	j51.51	-j.01941	j17.841	-j.0560	j8.005	-j.1249
.05	j20.64	-j.04843	j7.252	-j.1379	j3.4428	-j.2905
.1	j10.39	-j.09619	j3.819	-j.2619	j2.061	-j.4851
.2	j5.337	-j.1874	j2.227	-j.4490	j1.469	-j.6808
.5	j2.465	-j.4056	j1.417	-j.7057	j1.170	-j.8547
1.0	j1.639	-j.6098	j1.193	-j.8378	j1.082	-j.9240
2.0	j1.290	-j.7751	j1.093	-j.9150	j1.040	-j.9610
5.0	j1.108	-j.9023	j1.036	-j.9651	j1.010	-j.9840
10.0	j1.053	-j.9498	j1.018	-j.9824	j1.008	-j.9922

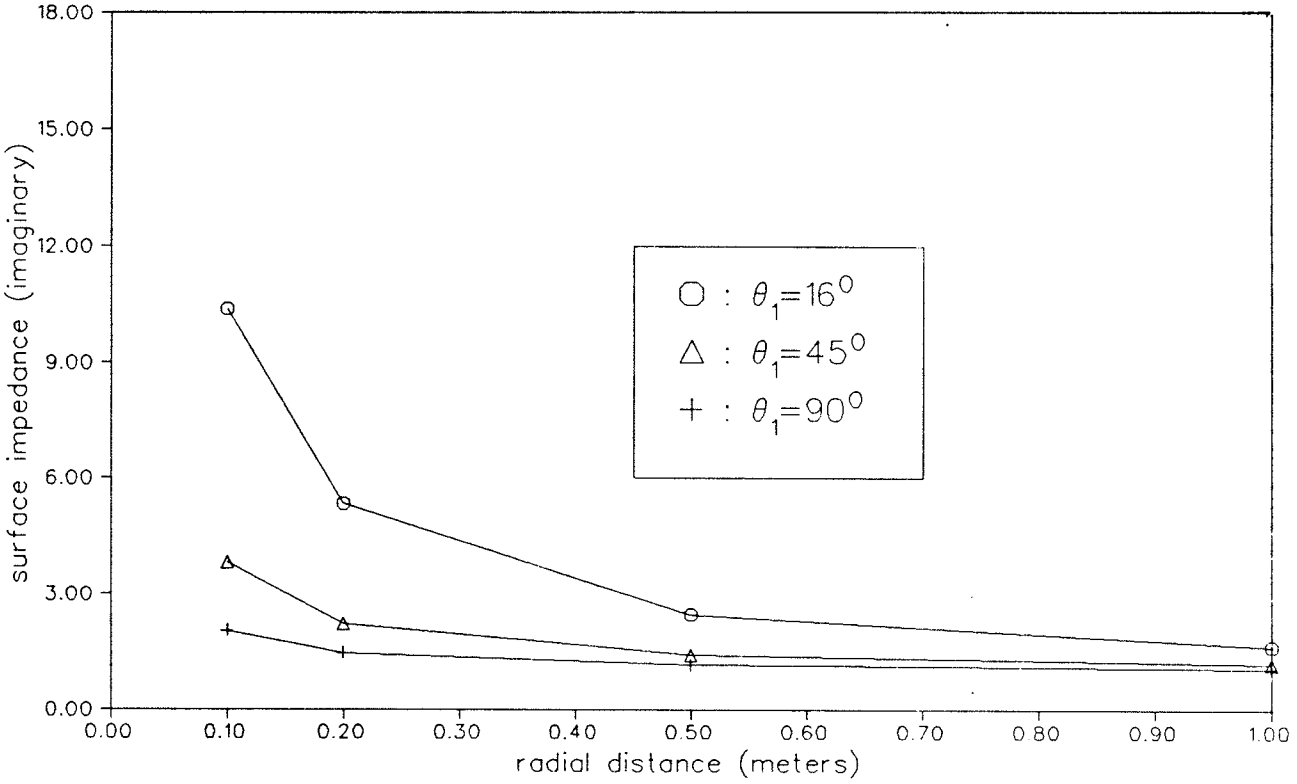

FIG 4.4: Graph of Surface Impedance vs Distance along Horn Wall
*N.B.– Surface impedances relative to free space value

Chapter 5 : DESIGN OF A DIELECTRIC LINED CONICAL HORN

The next logical step in this analysis is to attempt to develop a practical design for use as a hybrid mode feed. Dragone [1981] cites several structures which can be used to simulate a surface impedance in a waveguide. The first section of this chapter will review these structures and present a basic analysis. The next section uses a variable thickness dielectric lining to provide the neccessary surface impedance taper.

5.1 Surface Impedances

The idea of an equivalent surface impedance at an air-dielectric boundary was investigated by several authors. In a book by Collin [1960] both thick and thin dielectric sheets over perfectly conducting metal plates are discussed. In both cases, the analysis is accomplished by treating the dielectric slab as a transmission line and transforming the zero impedance condition at the dielectric-conductor interface to an approximate value at the air-dielctric interface. In this analysis the equivalent surface impedance at the air- dielectric interface is dependent on the angle of incidence, frequency and polarisation of the incoming wave and the permittivity, permeability and thickness of the dielectric.

Wait [1962] has investigated the surface impedance of a multi- layered space in order to investigate propagation over the earth's surface. He presents numerical results for several situations using lossy dielectric layers. In the two layer case, Wait [1964 p.54] shows that if the argument, $(\sigma \mu \omega)^{\frac{1}{2}} h_1$, is greater than about 3, the amplitude of the surface impedance is equal to unity and the phase is zero. In this case, h_1 is the thickness of the dielectric layer and σ is the conductivity of the dielectric. Thus, the effect of the conductor on the surface impedance gradually decreases as the thickness of the layer increases. It can also be seen that the surface impedance does not vary wildly as a function of dielectric thickness, as is

the case with the lossless layer.

It must be remembered that even if the problem of the equivalent surface impedance has been solved for a flat surface it is not neccessarily valid to apply this situation to the interior of a waveguide. Waldron [1969] warns that the only sure method of finding the equivalent surface impedance of a dielectric/metal structure is to solve the boudary value problem exactly and then take the ratio of the appropriate E and H fields at the air-dielectric surface. Waldron goes on to comment that there are situations where the surface impedance boundary conditions can be used to solve a waveguide problem. He verifies that the surface impedance model will work for a circular waveguide with dielectric lining if the impedance of the lining is taken to be the same as the impedance of an equivalent thickness of dielectric over a plane metallic plate. Dragone [1981] has used this method to solve for the fields in a large diameter, narrow flare-angle conical horn. By choosing the thickness of the dielectric carefully the cone can be made to support hybrid modes.

To obtain the surface impedance taper neccessary to satisfy the conditions set forth in section 4.4 it was assumed that the surface impedance model used by Dragone was applicable. This may not, in fact, be the case but in order to find the exact expression for the surface impedance it would be neccessary to solve the boundary value problem in both regions. This boundary value problem has been solved but only in terms of a radial eigenfunction expansion which is not easily applicable to the angular eigenfunction approach taken here [Hadidi 1985]. An obvious extension of this work, one that would encompass this work and many others, would be to solve the boudary value problem to find simple expressions for the field in a dielectric lined conical waveguide.

5.2 Tapered Surface Impedance

The neccessary surface impedance taper to support the hybrid modes in a dielectric lined conical waveguide is given from section 4.4 by;

$$\eta_{\pm} = -\frac{P}{P'}\frac{\nu(\nu+1)}{2\eta_0 R}\frac{1}{j\omega\sin\theta_1\epsilon_0} \pm \left(\frac{-P^2}{(P')^2}\frac{\nu^2(\nu+1)^2}{4\eta_0^2R^2}\frac{1}{\omega^2\sin^2\theta_1\epsilon_0{}^2}-1\right)^{\frac{1}{2}} \quad (5.2.1)$$

The present task is to find methods of achieving this taper in practice.

The use of tapered surface impedances has been applied to this type of problem in the past. Felsen [1959] wrote a general paper which used a linearily tapered surface impedance to simplify the problem of scattering from lossy cones and wedges. Bahar [1967] has also used a linearly varying surface impedance to simplify the analysis for a conical waveguide. Although neither of these works include hybrid mode analysis it is important to note the precedent set by these papers. Neither of the above two authors offered any methods for obtaining the desired surface impedance taper physically.

The model used to simulate the surface impedance of a dielectric slab over the top of a metal surface is taken from Dragone's paper on waveguides [Dragone 1981]. The general situation is shown in Fig. 5.1 for a three-layered sandwich of dielectric and metal. For this particular application the upper dielectric is taken to be air. The expressions for the impedance in the radial and the roll directions are;

$$Z_R = j\, r_{21}\frac{n_1}{n_2}\eta_0 T + R_s(1+T^2) \quad (5.2.2)$$

$$Z_\phi = j\frac{1}{r_{21}}\frac{n_1}{n_2}\eta_0 T + R_s(1+T^2) \quad (5.2.3)$$

where;

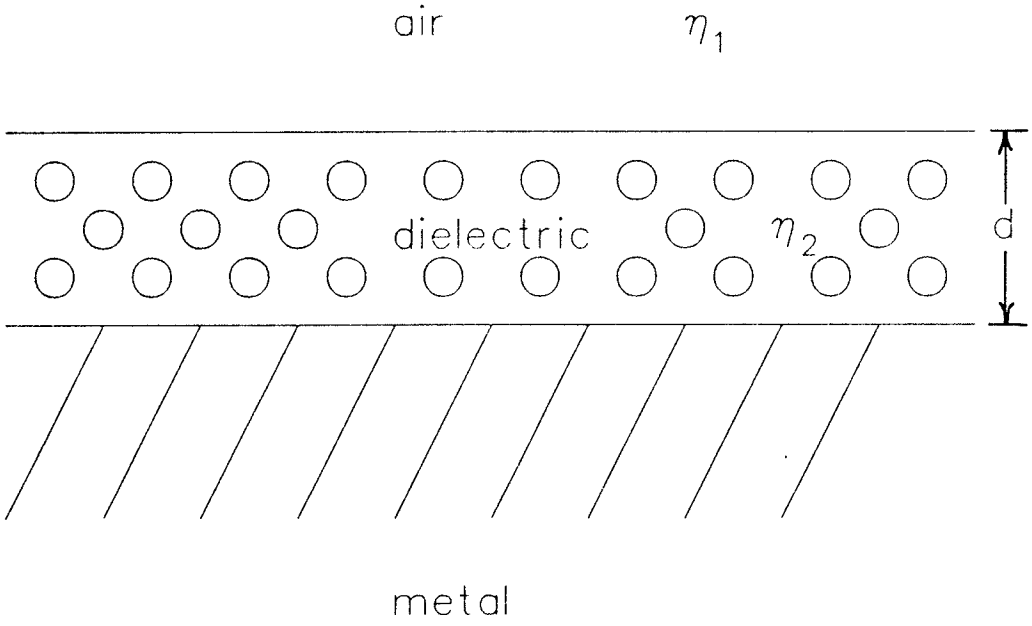

Fig. 5.1 :
Diagram of a Dielectric
Coating on a Metallic Wall

$$T = tan\left(K_0 \sqrt{n_2^2 - n_1^2}\, d\right)$$

$$\eta_0 = \sqrt{\frac{\mu_0}{\epsilon_0}}$$

$$r_{21} = \frac{\sqrt{n_2^2 - n_1^2}}{n_2} \ .$$

In the above equations, n_1 and n_2 are the respective indices of refraction for each dielectric, K_0 is the wave impedance of free space and these expressions are valid for $\frac{R_s}{Z} << T, \frac{1}{T}$. R_s is the resistivity of the conducting wall. This condition is certainly met by assumming $R_s = 0$ as would be applicable to a perfectly conducting metal wall. This simplifies Eqns. (5.2.2) and (5.2.3) to obtain;

$$Z_R = j\ r_{21}\ \frac{n_1}{n_2}\ \eta_0\ T \qquad (5.2.4)$$

$$Z_\phi = j\ \frac{1}{r_{21}}\ \frac{n_1}{n_2}\ \eta_0\ T \ . \qquad (5.2.5)$$

This thesis has assumed that the central cone of dielectric is air, therefore $n_1 = 1.0$. A further simplification to the wall impedances is to assume that $n_2^2 >> n_1^2 = 1.0$. Under this condition the two impedances are equal and can be written as;

$$Z_R = Z_\phi = j\frac{1}{n_2}\ \eta_0\ T \ . \qquad (5.2.6)$$

Equation (5.2.5) is very useful for the present purpose. It is possible under the above approximations to simulate the impedance surface by varying the thickness of the dielectric. There is, however, one disadvantage to this type of simulation. Since the inner surface of the dielectric was assumed to be in the shape of a cone (i.e. with straight walls) it is the surface at the metal dielectric interface

which must be curved to accomodate the changing thickness of the dielectric lining. Figure 5.2 displays the general shape of the structure which could support hybrid modes in a cone.

Another possible method of achieving the same results but using a constant thickness dielectric layer on the walls, is to vary the dielectric properties of the layer as a function of the radial distance. This may appear to be a more favourable solution since the dielectric structure could then be added to any standard conical horn with smooth walls in order to convert it to a hybrid-mode horn. This solution may not be very practical since the manufacturing of an insert with carefully tapered dielectric properties may be very difficult. This is certainly one area of interest for the commercial applications of this idea.

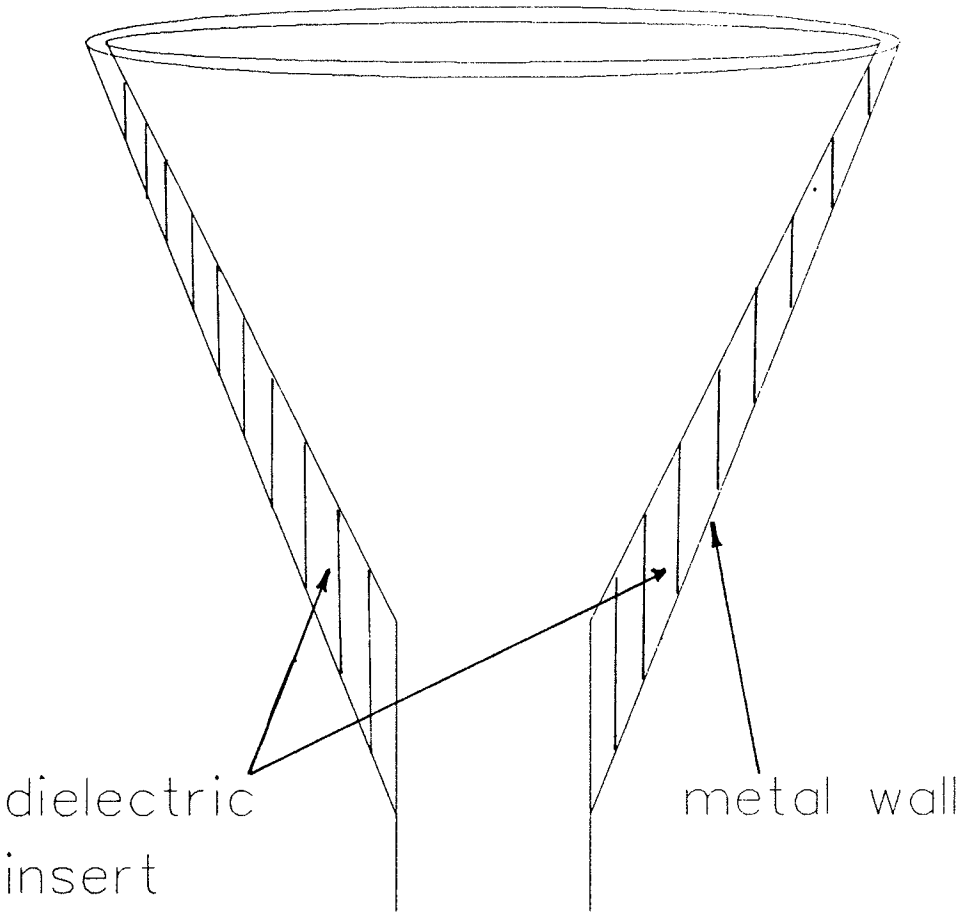

Fig. 5.2 : Conical Horn with a Tapered Dielectric Insert

Chapter 6 : RADIATION FROM A DIELECTRIC LINED HORN

Once the field distribution in the aperture of any horn is known it is a relatively simple procedure to obtain the far field radiation characteristics by employing the field equivalence principles.

The first section of this chapter calulates and plots the aperture field distributions for the $\phi=0^o$ case for the first three HE_{1n} and EH_{1n} modes. The radiated fields for these modes are then presented in the second section along with a brief description of how these radiation patterns were calculated.

6.1 Aperture Field Distribution

In section 4.3 the aperture fields due to spherical hybrid modes were analysed. The aperture field for the $\phi=0^o$ plane is,

$$E_\phi = \bar{\Lambda} J_1'(q\theta) + \frac{\bar{\beta} J_1(q\theta)}{q\theta} \tag{6.1.1}$$

and for the $\phi=90^o$ plane;

$$E_\theta = \bar{\beta} J_1'(q\theta) + \frac{\bar{\Lambda} J_1(q\theta)}{q\theta} \tag{6.1.2}$$

Figures 6.1 through 6.3 display the E-plane aperture fields ($\phi=0^o$ plane) for the first three HE_{1n} modes. Figures 6.4 through 6.6 do likewise for the first three EH_{1n} modes. Since the modes are assumed to be balanced hybrid modes, the H-plane ($\phi=90^0$) aperture distribution is identical to the E-plane distribution. These plots are for a large, hybrid mode conical antenna with an aperture diameter of 89 inches. The flare angle is assumed to be small so the aperture can be considered in cylindrical coordinates rather than spherical.

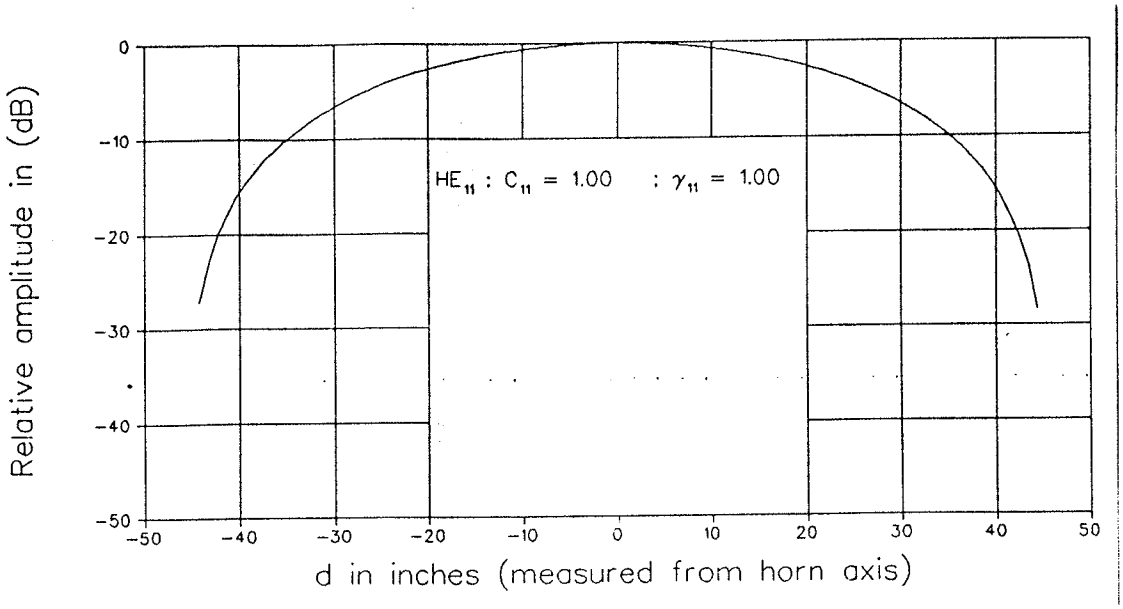

Fig. 6.1 : E-plane aperture field of the HE_{11} mode.

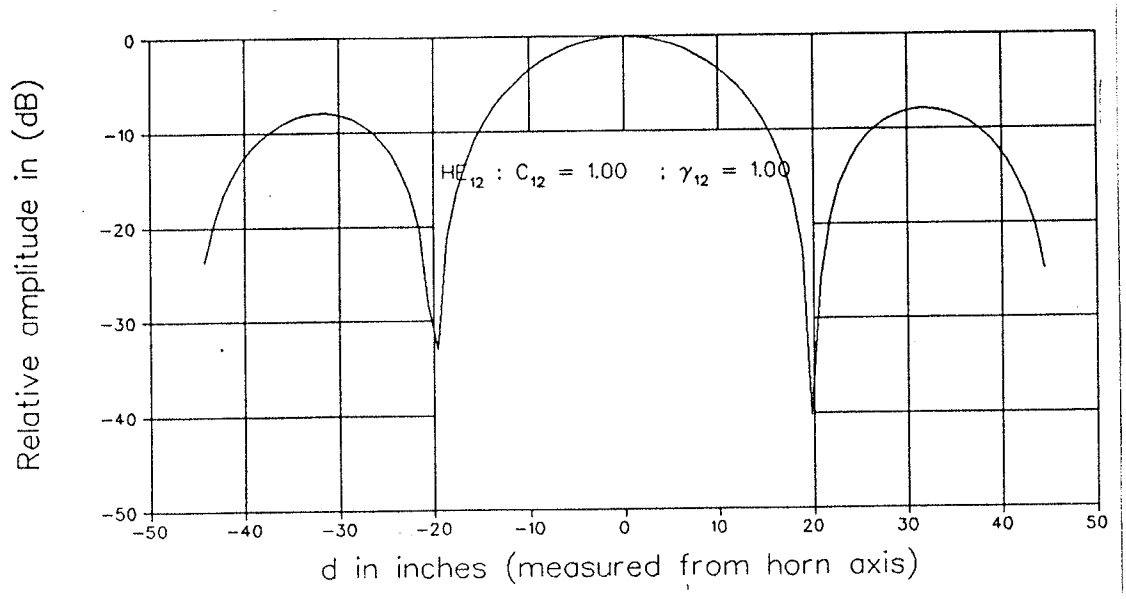

Fig. 6.2 : E-plane aperture field of the HE_{12} mode.

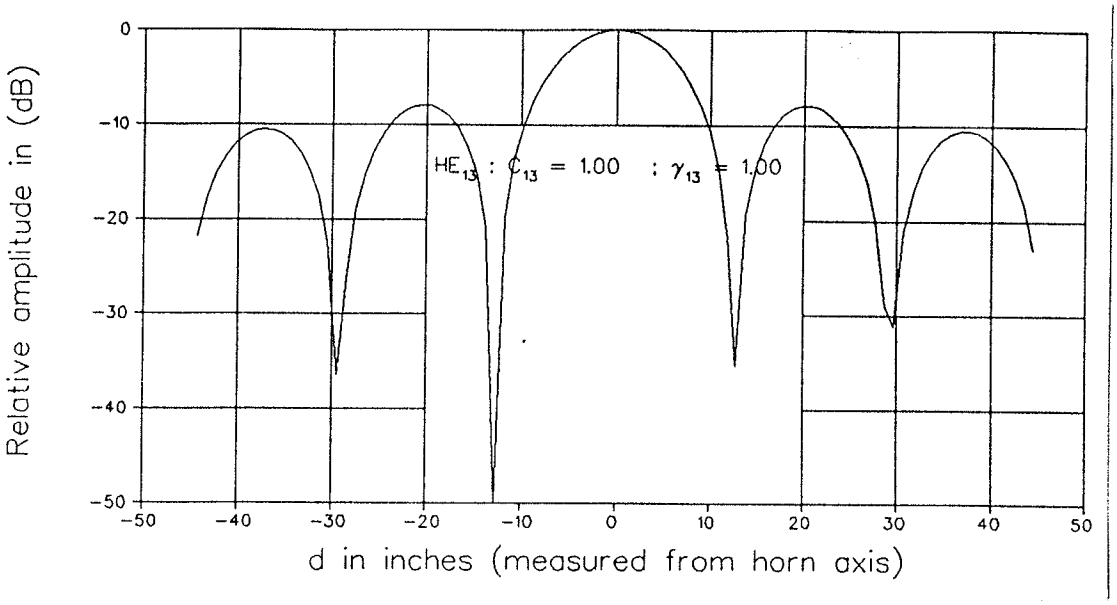

Fig. 6.3 : E-plane aperture field of the HE_{13} mode.

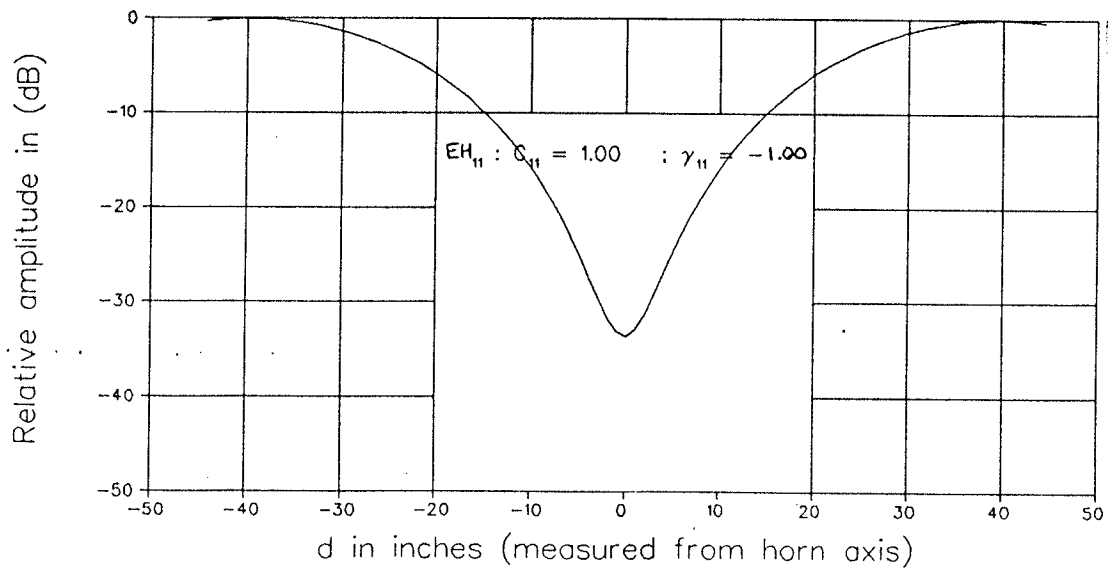

Fig. 6.4 : E-plane aperture field of the EH_{11} mode.

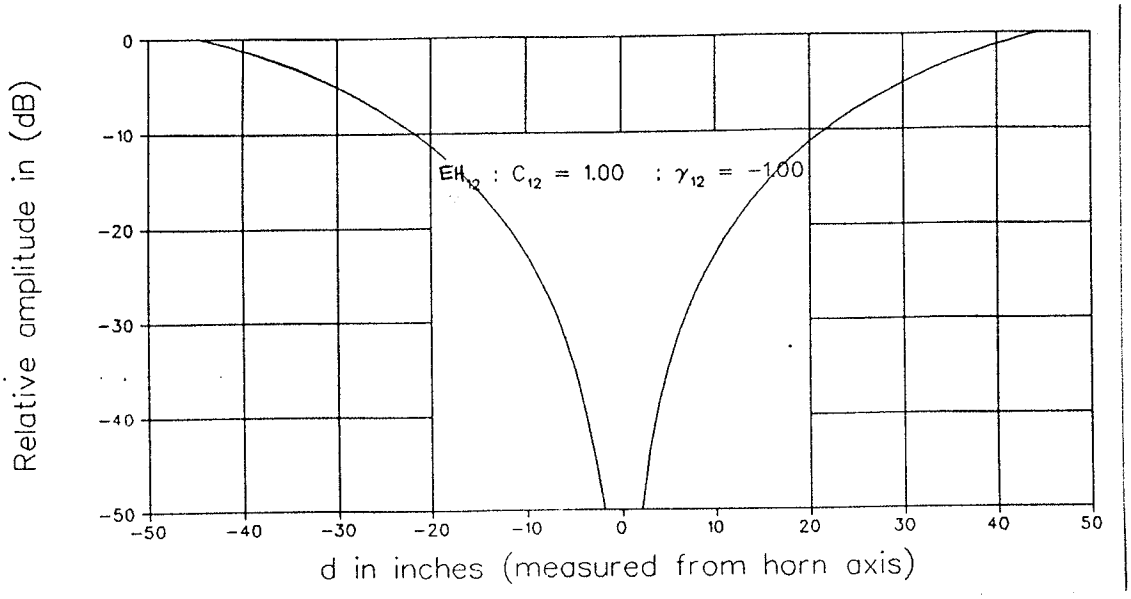

Fig. 6.5 : E-plane aperture field of the EH_{12} mode.

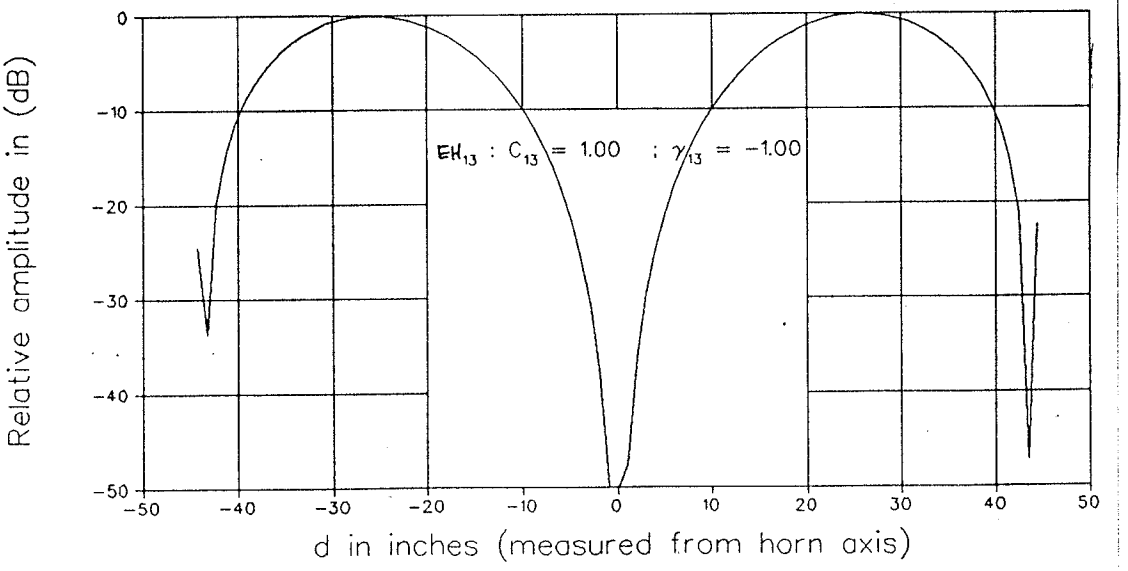

Fig. 6.6 : E-plane aperture field of the EH_{13} mode.

6.2 Radiated Fields from a Dielectric Lined Horn

The radiated fields from a specific aperture distribution can be found using the well known field equivalence principles. The vector potentials can be found from the equivalent electric and magnetic currents over the aperture as;

$$\bar{A}_e(r)=\frac{\mu_0}{4\pi}\int_S \bar{J}_e(r')e^{-jk_0R}dS' \tag{6.2.1}$$

$$\bar{A}_m(r)=\frac{\epsilon_0}{4\pi}\int_S \bar{J}_m(r')e^{-jk_0R}dS' \tag{6.2.2}$$

Figure 6.7 displays the coordinate system used in this analysis. The source is denoted by the primed coordinates and the far field by the unprimed; as is the standard convention.

Using the far field approximations for R, written below in equations (6.2.3) and (6.2.4);

$$R=r-r'\cos\psi \qquad \text{for } \textit{phase term} \tag{6.2.3}$$

$$R=r \qquad \text{for } \textit{amplitude term} \tag{6.2.4}$$

Eqs. (6.2.1) and (6.2.2) reduce to

$$\bar{A}_e(r)=\frac{\mu_0}{4\pi r}e^{-jk_0r}\ N \tag{6.2.5}$$

$$\bar{A}_m(r)=\frac{\epsilon_0}{4\pi r}e^{-jk_0r}\ L \tag{6.2.6}$$

where,

$$N=\int\int_S \bar{J}_e(r')e^{jk_0r'\cos\psi}dS'$$

$$L=\int\int_S \bar{J}_m(r')e^{jk_0r'\cos\psi}dS' .$$

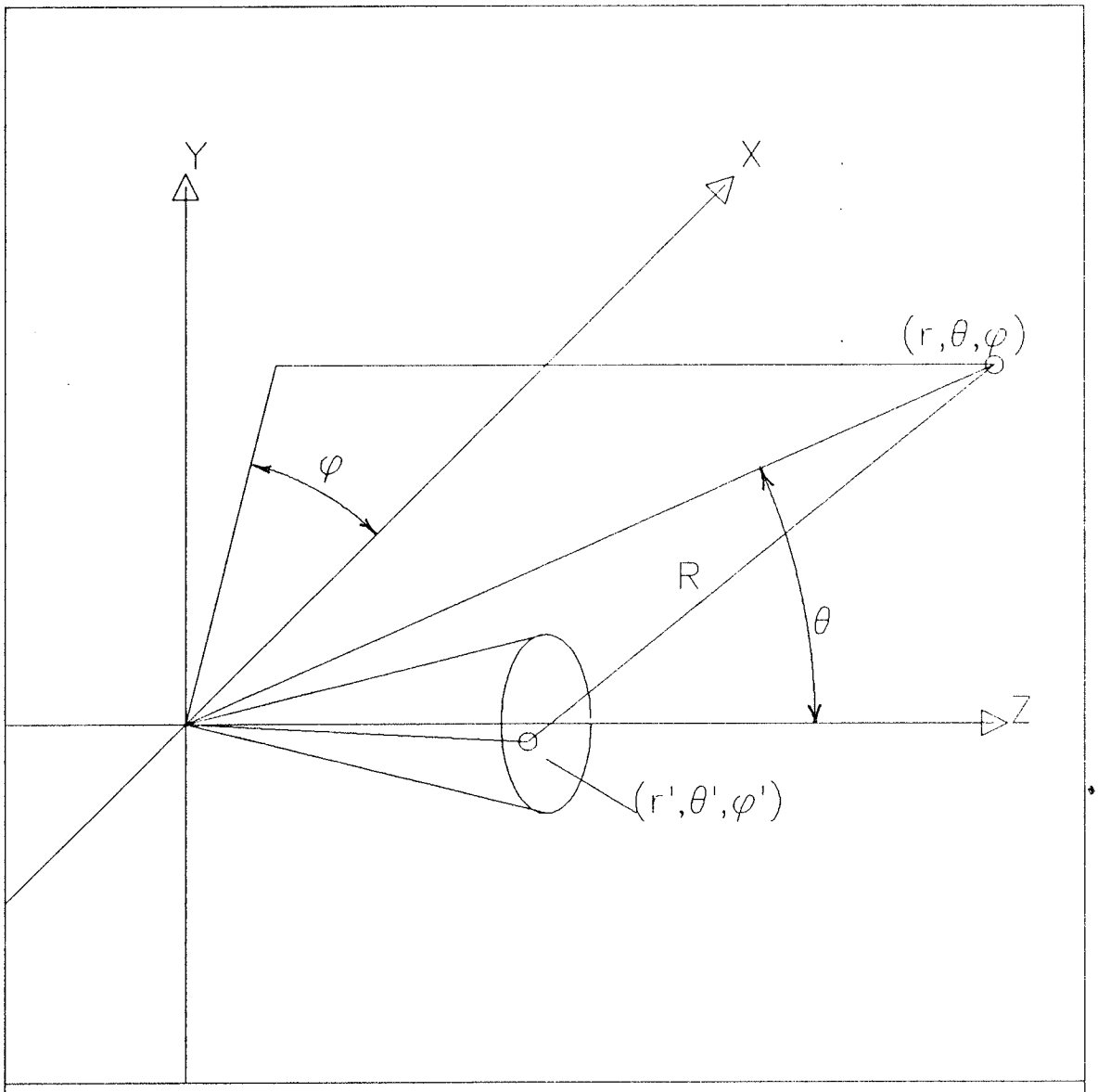

Fig. 6.7 :
Coordinate System
Used in the Analysis

In the radiation zone the expressions for the electric and magnetic fields can be found from the potentials as;

$$E_r = 0 \tag{6.2.7}$$

$$E_\theta = -\frac{jk_o e^{-jk_o r}}{4\pi r}(L_\phi + \eta N_\theta) \tag{6.2.8}$$

$$E_\phi = \frac{jk_o e^{-jk_o r}}{4\pi r}(L_\theta - \eta N_\phi) \tag{6.2.9}$$

$$H_r = 0 \tag{6.2.10}$$

$$H_\theta = \frac{jk_o e^{-jk_o r}}{4\pi r}(N_\phi - \frac{L_\theta}{\eta}) \tag{6.2.11}$$

$$H_\phi = -\frac{jk_o e^{-jk_o r}}{4\pi r}(N_\theta + \frac{L_\phi}{\eta}) \; . \tag{6.2.12}$$

For a flat aperture, the expressions for N and L can be written in terms of Cartesian coordinates as;

$$N_\theta = \int\int_S [J_x \cos\theta\cos\phi + J_y \cos\theta\sin\phi - J_z \sin\theta] e^{jk_0 r' \cos\psi} dS' \tag{6.2.13}$$

$$N_\phi = \int\int_S [-J_x \sin\phi + J_y \cos\phi] e^{jk_0 r' \cos\psi} dS' \tag{6.2.14}$$

$$L_\theta = \int\int_S [M_x \cos\theta\cos\phi + M_y \cos\theta\sin\phi - M_z \sin\theta] e^{jk_0 r' \cos\psi} dS' \tag{6.2.15}$$

$$L_\phi = \int\int_S [M_x \sin\phi + M_y \cos\phi] e^{jk_0 r' \cos\psi} dS' \; . \tag{6.2.16}$$

A transformation of coordinates is neccessary to apply these expressions to the spherical aperture of the conical horn. The alternative option would be to use a cylindrical aperture model for the conical horn and account for the spherical phase front by modifying the phase of the aperture distribution. It was decided

that using the spherical aperture method was more useful since the transformation of the radiation integrals to spherical coordinates would be applicable to other problems and may be useful in future work. The expressions for the radiation integrals from a spherical aperture are presented below.

$$N_\theta = \int\int J_r (\sin\theta' \cos\theta \cos(\phi-\phi') - \cos\theta' \sin\theta)$$

$$+J_\theta (\cos\theta' \cos\theta \cos(\phi-\phi') + \sin\theta \sin\theta') + J_\phi (\cos\theta \sin(\phi-\phi'))$$

$$e^{jkr' \sin\theta' \sin\theta \cos(\phi-\phi') + \cos\theta \cos\theta' r'^2} \sin\theta' \, d\theta' \, d\phi' \qquad (6.2.17)$$

$$N_\phi = \int\int -J_r (\sin\theta' \sin(\phi-\phi') - J_\theta \cos\theta' \sin(\phi-\phi') + J_\phi \cos(\phi-\phi')$$

$$e^{jkr' \sin\theta' \sin\theta \cos(\phi-\phi') + \cos\theta \cos\theta' r'^2} \sin\theta' \, d\theta' \, d\phi' \qquad (6.2.18)$$

Identical expressions are obtained for L_θ and L_ϕ by replacing J by M in the above two equations.

These expressions were utilized to generate the radiation patterns shown in Figs. 6.8 through 6.13. Since the fields corresponding to the HE modes in the conical structure are largely concentrated in the center of the aperture it was expected that the contribution of the fields diffracted from the edges of the horn will be negligible when compared to the radiated fields. This is not true of the EH modes since these modes have a large field at the walls of the horn. The diffracted field from the edges of the horn was not computed into the far field plots for two reasons. Firstly, the edge of this structure is not a simple metal edge but a metal edge covered partially by dielectric. In this case it is somewhat more difficult to calculate the diffracted field unless a model for the fields inside the dielectric lining is found. This is one area of future work which could be continued. The second reason is that most applications of hybrid-mode horns utilize only the HE_{11} mode; the EH modes and higher order HE modes being

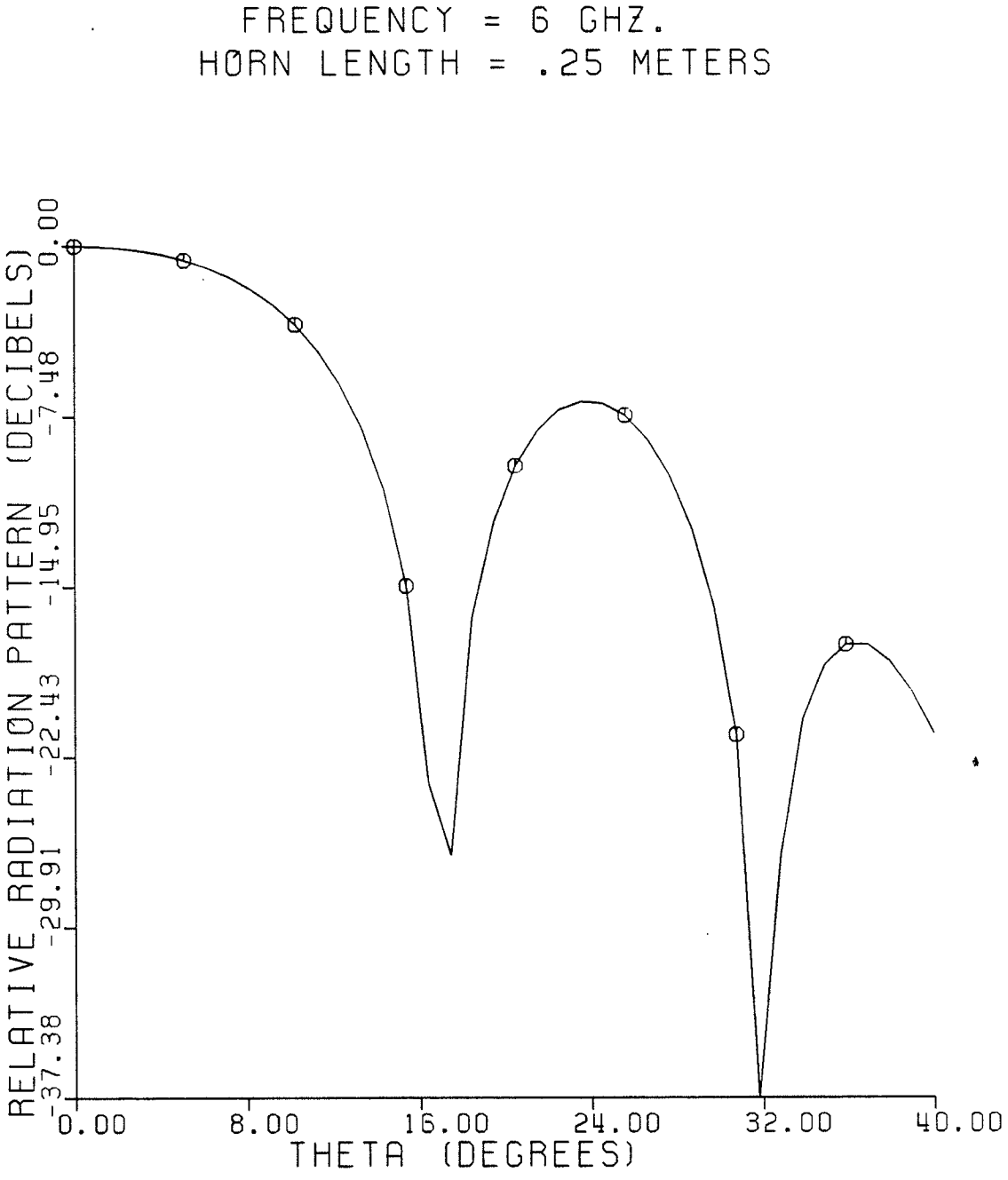

Fig. 6.8 : E-plane plot of the far field of the balanced HE_{11} mode.

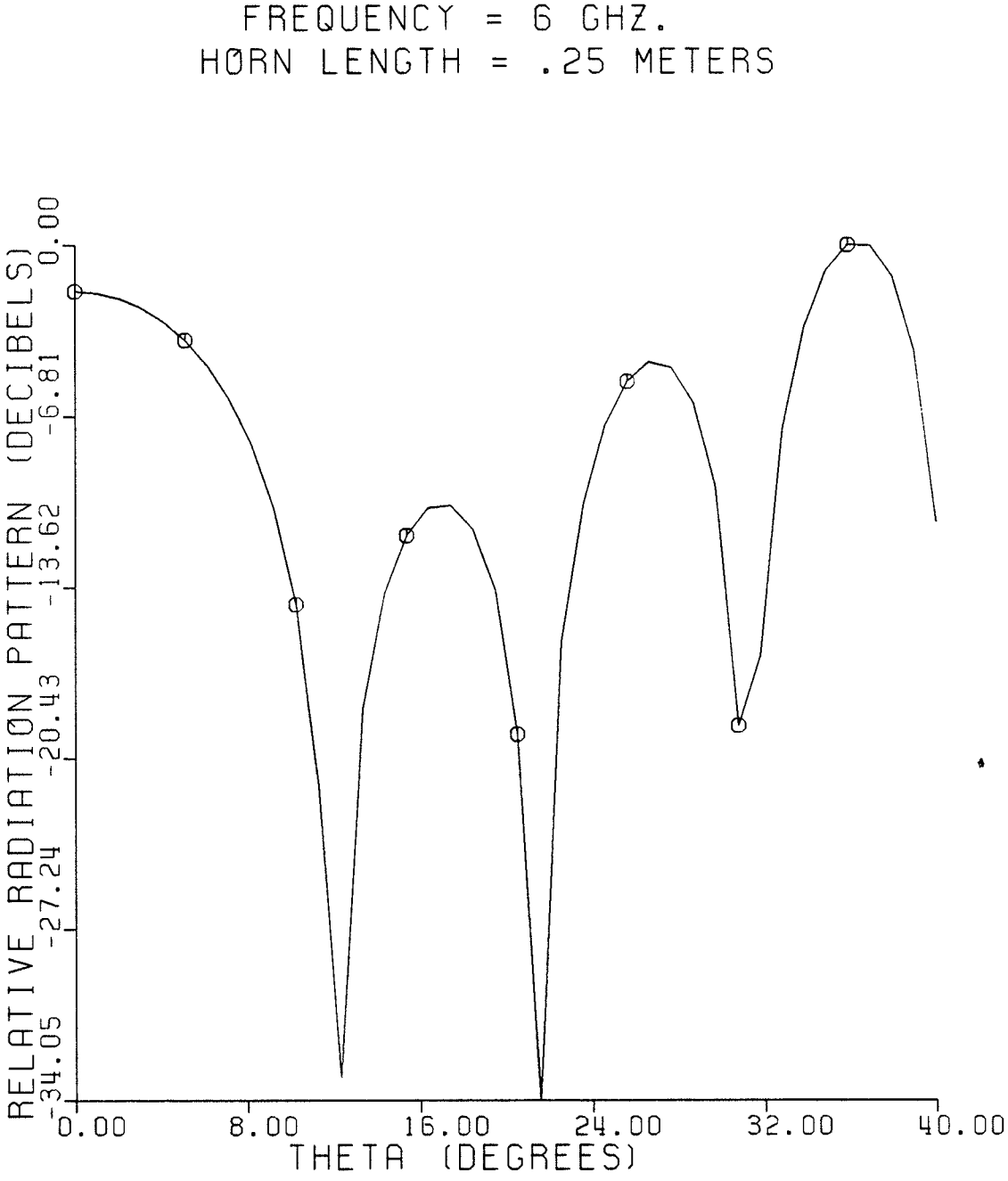

Fig. 6.9 : E-plane plot of the far field of the balanced HE_{12} mode.

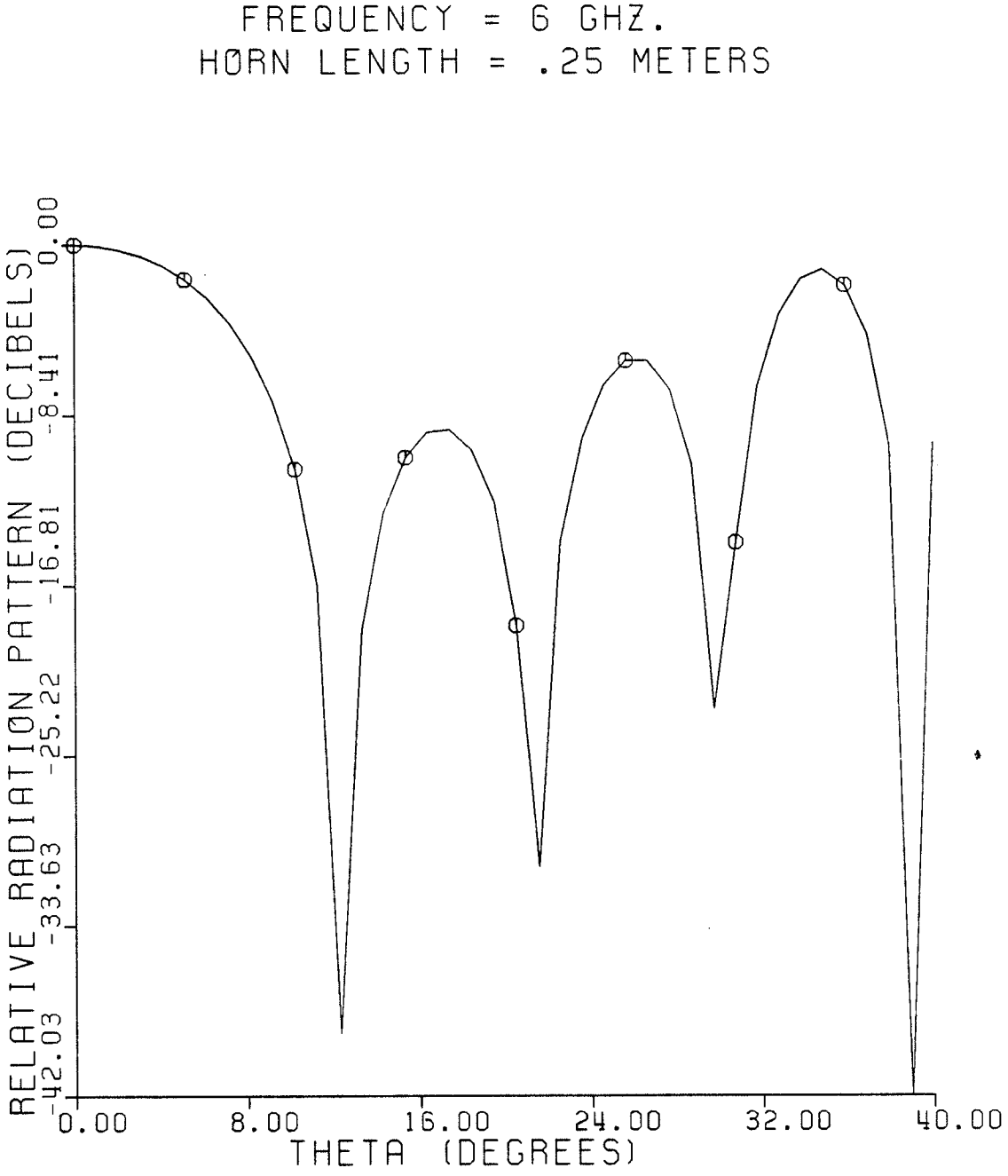

Fig. 6.10 : E-plane plot of the far field of the balanced HE_{13} mode.

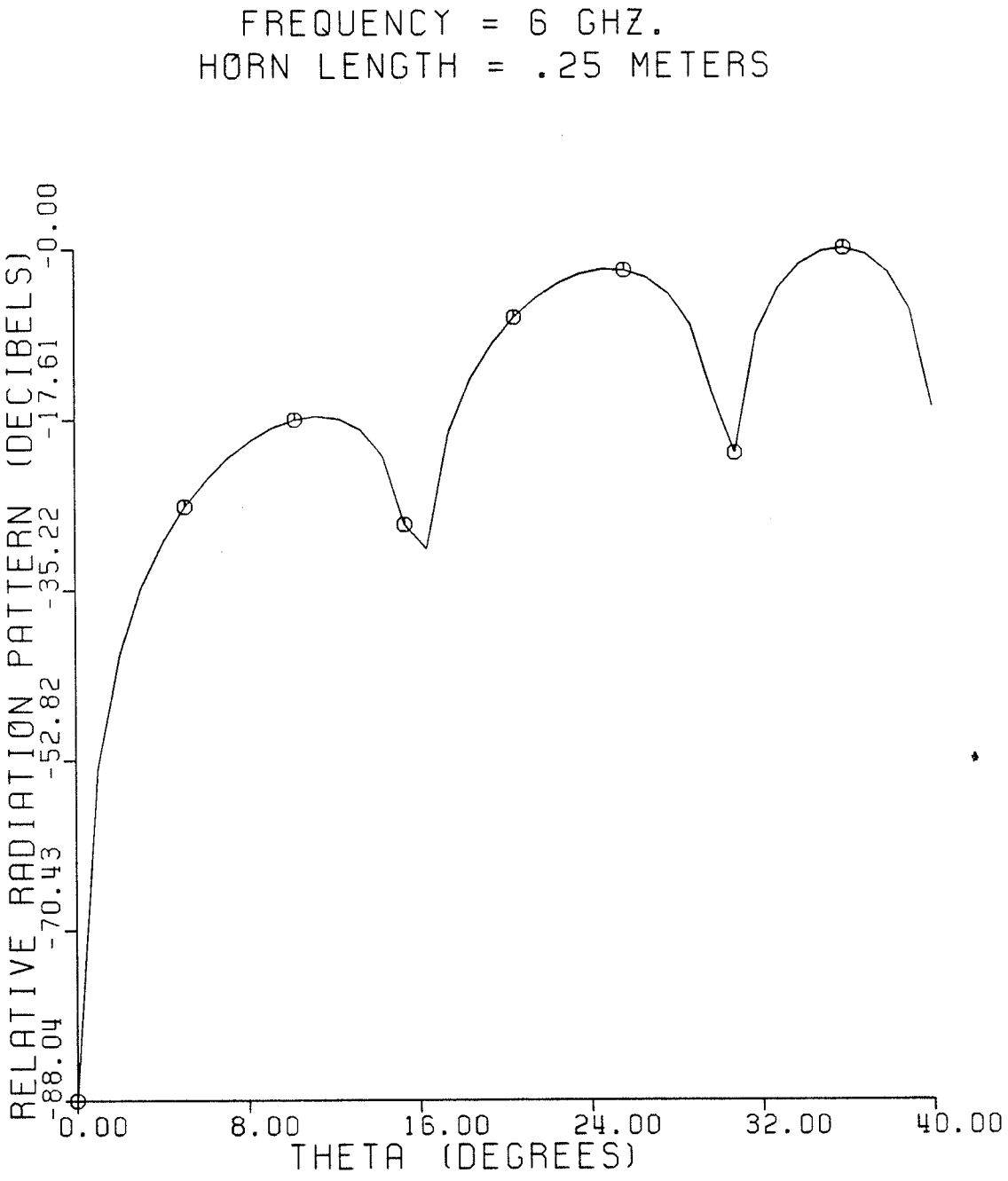

Fig. 6.11 : E-plane plot of the far field of the balanced EH_{11} mode.

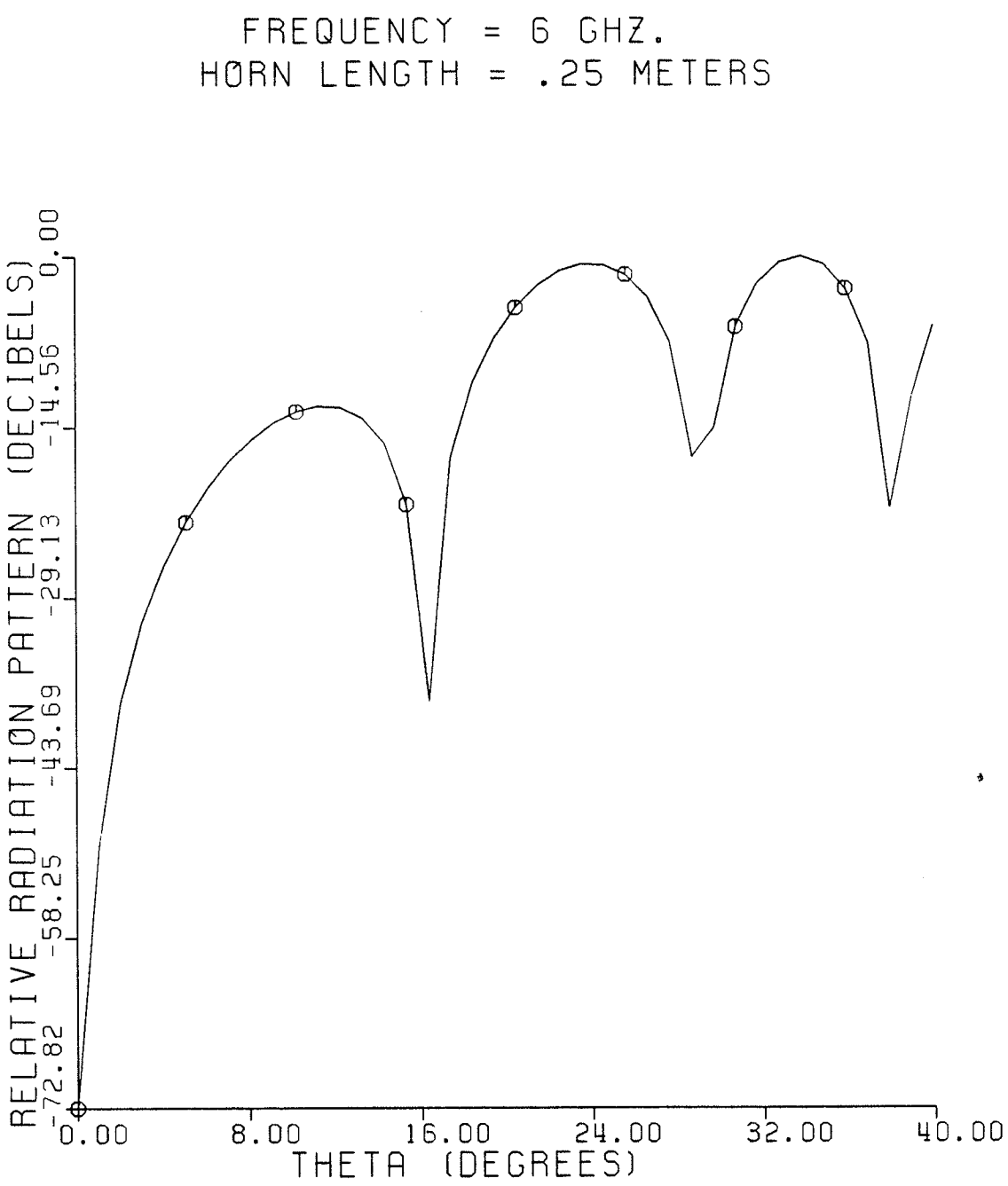

Fig. 6.12 : E-plane plot of the far field of the balanced EH_{12} mode.

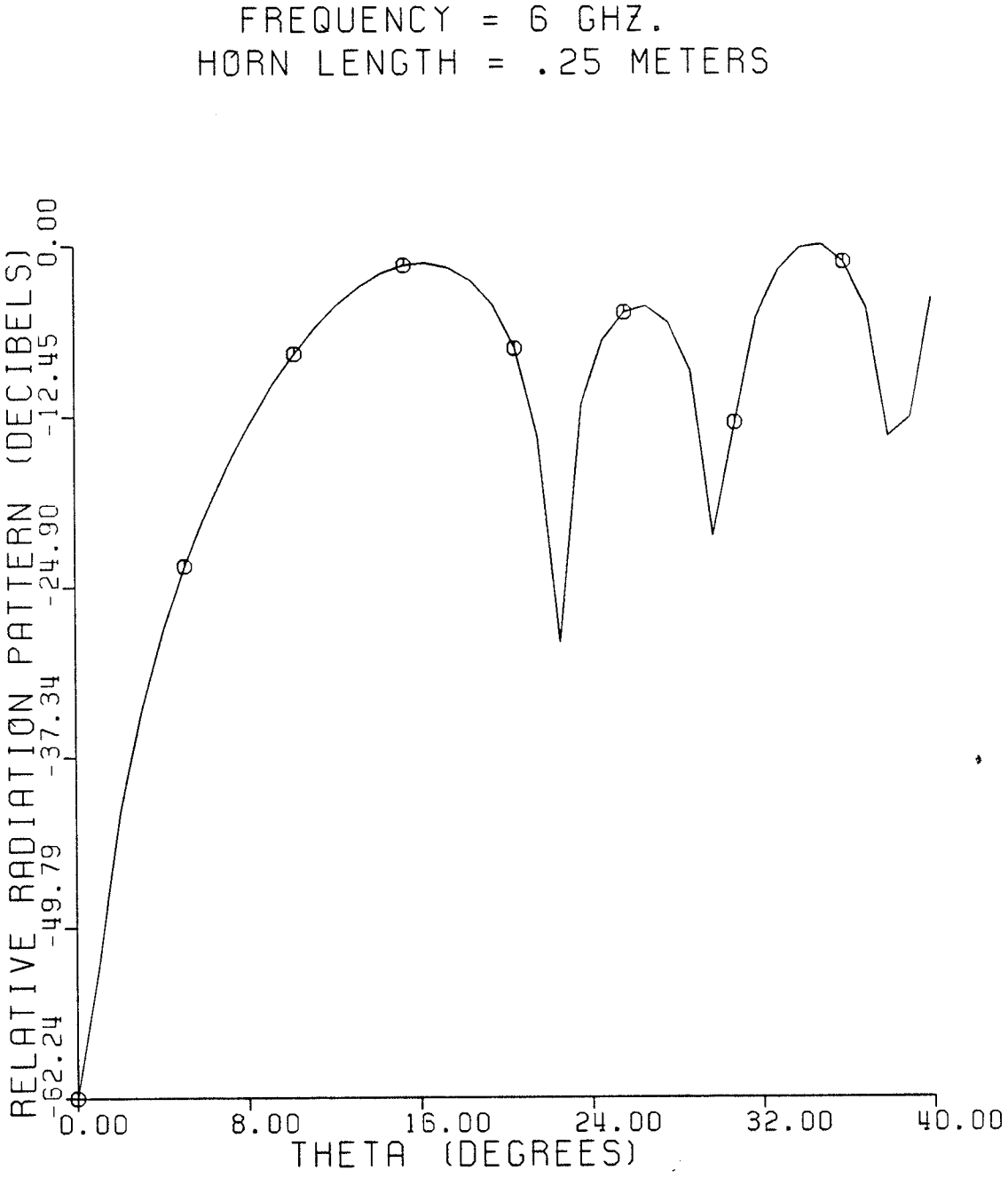

Fig. 6.13 : E-plane plot of the far field of the balanced EH_{13} mode.

undesirable. Thus, these radiation patterns provide a first order approximation which is useful in gaining a fundamental understanding of the behavior of each type of mode. In comparing the theoretical plots with previously published experimental plots it was found that the effect of diffraction can indeed be important, especially in small aperture horns. The sharp nulls in the experimental plots are masked by contributions from diffraction at the edges of the horn in the experimental plots.

Figure 6.14 shows the E and $H-plane$ fields of a smooth-walled conical horn given in a paper by Potter [1963] for a horn with a half-flare angle of 6.25^0, an aperture radius of 7.3 $cm.$ and at a frequency of 9.6 GHz. The comparison in this figure between the theoretical and measured plots points out the deficiencies in the aperture integration method. For comparison, Fig. 6.15 shows the far field as calculated by the aperture integration method of a conical horn of the same dimensions as in Fig. 6.14 but with hybrid-mode excitation. Both of these patterns (figs. 6.14 and 6.15) have a similar envelope, however, the symmetry of the patterns of the hybrid-mode feed make it a better choice for high performance applications. The sidelobes in the experimental curve of Fig. 6.14 are at about -18 $dB.$, or about 7 $dB.$ above the values predicted in the theoretical curves. If this same 7 $dB.$ factor is applied to the plots in Fig. 6.15 then a sidelobe level of less than -25 $dB.$ is predicted for a hybrid-mode horn; an improvement over the smooth-walled horn.

A further comparison was done for a horn with a half-flare angle of 15^0, a length of 21 $cm.$ and at a frequency of 7.4 GHz. Figure 6.16 is a previously published result by Jeuken [1969]. Figure 6.17 is the result obtained by the aperture integration technique. It was found that the envelope of the theoretical plot of Fig. 6.17 approximates the measured plot of Fig. 6.16 quite closely except for the nulls.

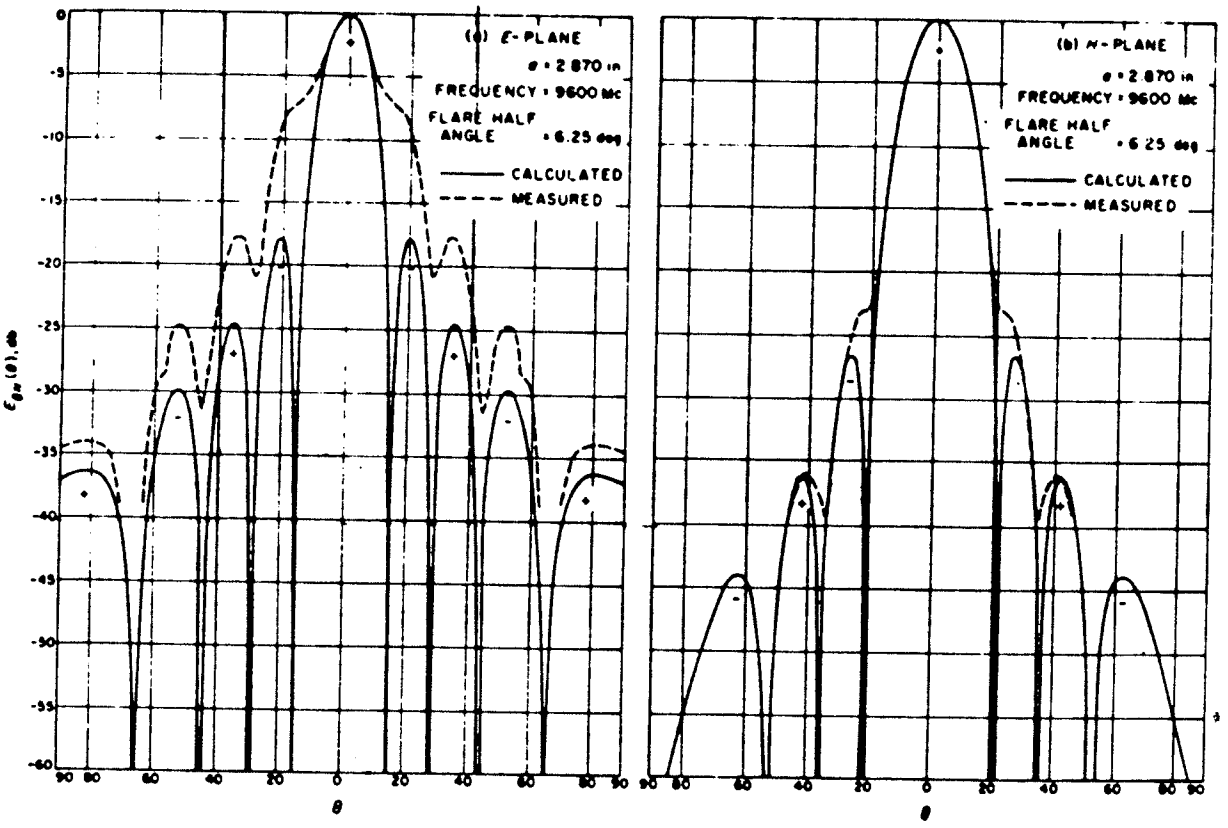

Fig. 6.14 : Theoretical and measured E and H- plane plots of the far field of the TE_{11} mode. (from [Potter 1963]).

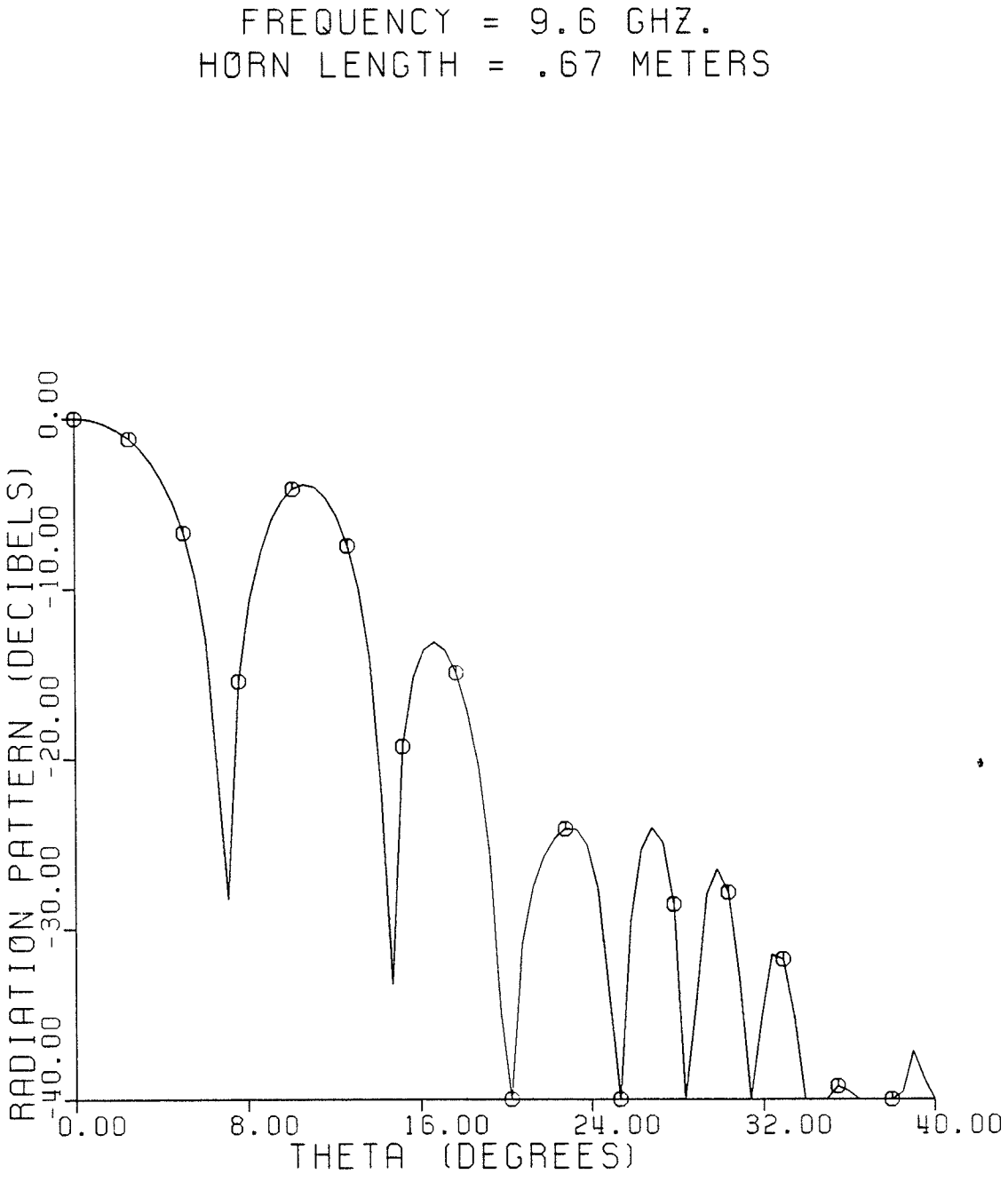

Fig. 6.15 : Theoretical E-plane plot of the far field of the balanced HE_{11} mode (half-flare angle = 6.25^0).

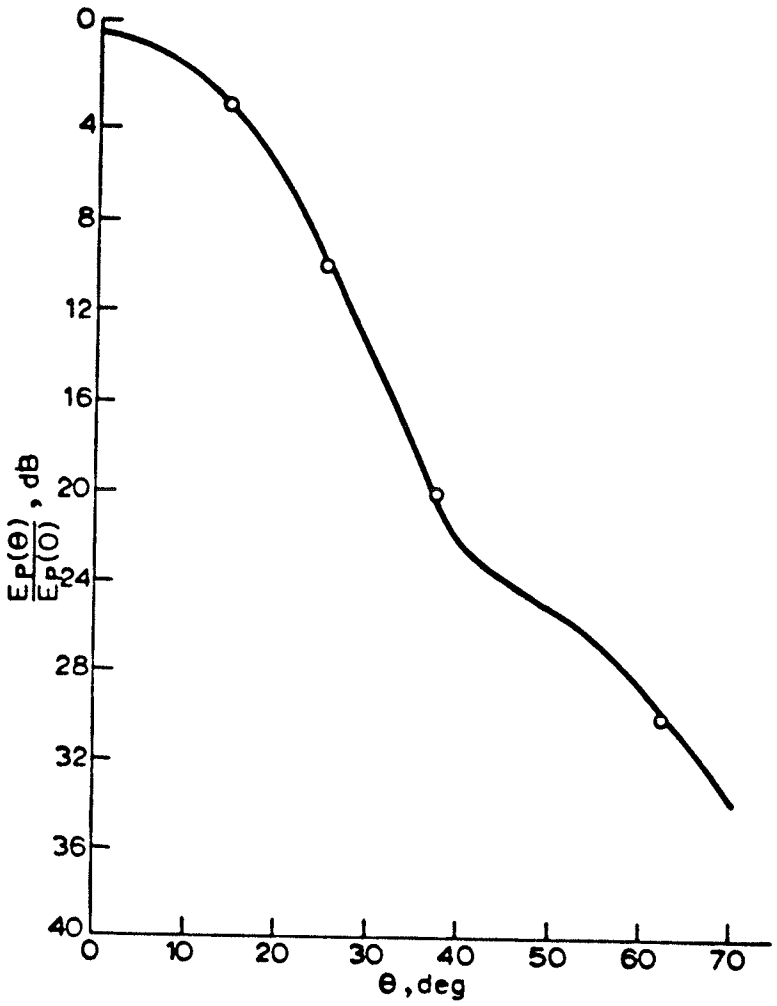

Fig. 6.16 : Measured E-plane plots of the far field of the balanced HE_{11} mode (from [Jeuken 1969]).

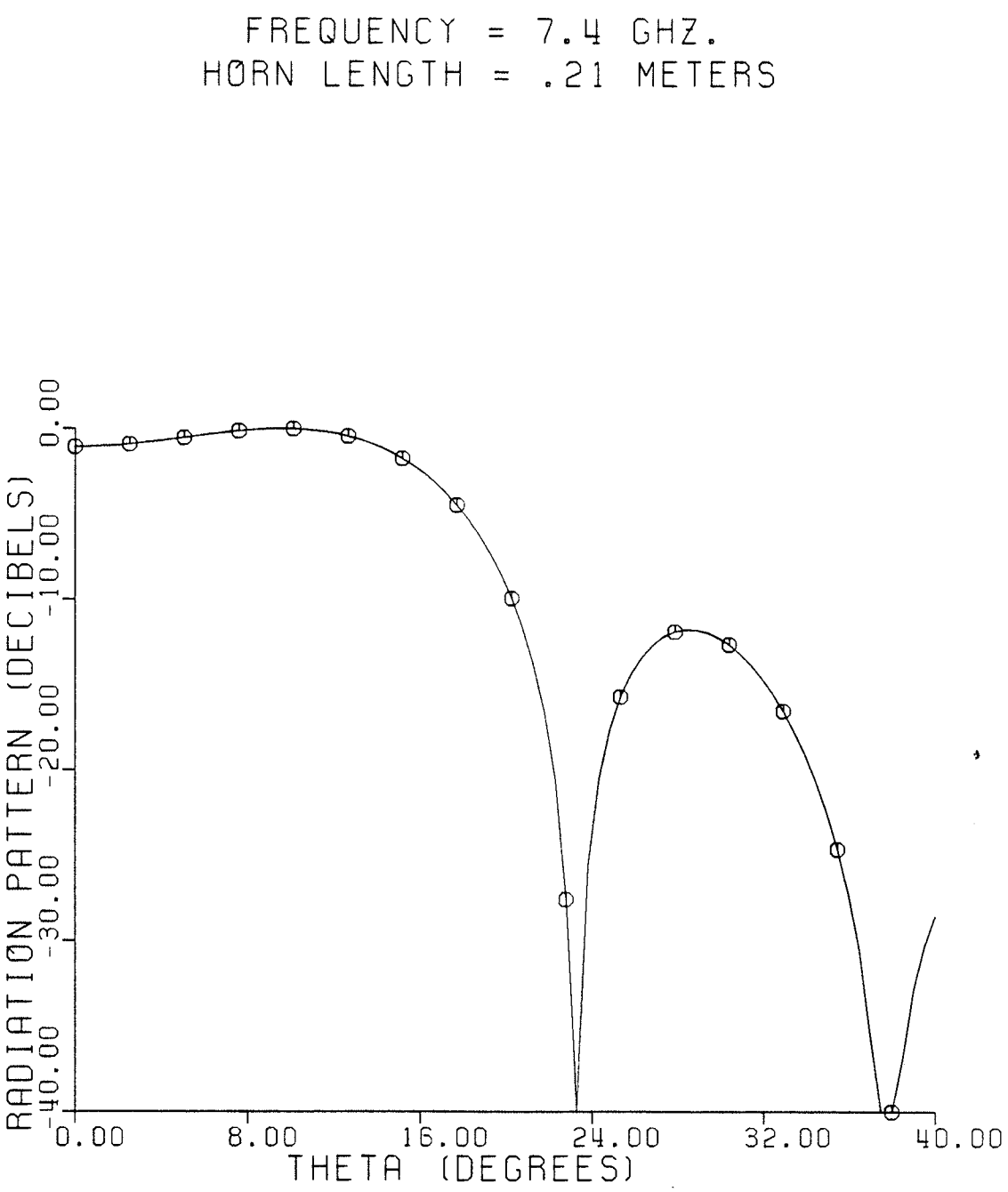

Fig. 6.17 : Theoretical E-plane plot of the far field of the balanced HE_{11} mode (half-flare angle = 15^0).

CONCLUSIONS

This thesis presents the analysis of circular cylindrical waveguide for the general case of an impedance boundary at the wall of the waveguide. It was found that hybrid modes exist in circular waveguide provided that the wall impedance is not zero or infinity. These modes will approach the balanced state as the radius of the waveguide is increased. For the special case of the wall impedances in the two tangential directions being reciprocal and the normalized impedance in the radial (Z) direction being equal to approximately 2.404, the eigenvalue of that mode is that of the balanced HE_{11} mode even for small diameter waveguides.

In the case of the conical waveguide with a constant impedance wall it was found that this waveguide will not support the hybrid modes that are associated with the corrugated waveguide. In order to satisfy the same characteristic equation as in the analysis of the corrugated waveguide it was found that it was neccessary to taper the impedance of the wall as a function of radial distance along the waveguide.

REFERENCES

* Agarwal, K.K. and Nagelberg, E.R.: "Phase characteristics of a circularly symmetric, dual-mode transducer." *IEEE Trans. Micro. Theo. Tech.*, MTT-18, January 1970, pp 69-71.

* Bahar, E. 'Generalized scattering matrix equations for waveguide structures for varying surface impedance boundaries' *Radio Science* , Vol. 2, (new series), No. 3, March 1967, pp. 287-297.

* Bryant, G.H.; "Propagation in Corrugated Waveguides", *Proc. IEE*, Vol. 116, No. 2, February 1969, pp. 203-213.

* Clarricoats, P.J.B., and Taylor, B.C.; "Evanescent and propagating modes of dielectric-loaded circular waveguide", *Proc. IEE*, Vol. III, 1964, pp. 1951-1956.

* Clarricoats, P.J.B., and Salema C.E.R.C.: 'Antennas employing conical dielectric horns, Part 1- Propagation and radiation characteristics of dielectric cones.' *Proc. IEE*, Vol. 120, No. 7, July 1973, pp.741-749.

* Clarricoats, P.J.B., and Salema C.E.R.C.: 'Antennas employing conical dielectric horns, Part 2- The Cassegrain Antenna.' *Proc. IEE*, Vol. 120, No. 7, July 1973, pp.750-756.

* Clarricoats, P. J. B. and Saha, P. K.: 'Propagation and radiation behavior of corrugated feeds, Part 2- Corrugated-conical-horn feed.' *Proc. IEE*, Vol. 118, No. 9, September, 1971, pp.1177-1186.

* Clarricoats,P.J.B.: 'Analysis of spherical hybrid modes in a corrugated conical horn.' *Electron. Lett.*, Vol. 5, May 1, 1969, pp. 189-190.

* Clarricoats, P.J.B. and Olver, A.D., **Corrugated horns for microwave antennas.** Peter Peregrinus Ltd., IEE series, London 1984, pp. 24-26.

* Collin, R.E.; **Field Theory of Guided Waves,** McGraw-Hill, U.S., 1960.

* Collin, R.E., **Antennas and Radiowave Propagation** McGraw-Hill,U.S.,1985.

* Dybdal, R.B., Peters, L.Jr. and Peake, W.H.; "Rectangular Waveguide with Impedance Walls"; *IEEE Trans. Micro. Theo. Tech.* Vol. MTT-19,No. 1,January, 1971. pp.2-9.

* Dragone, C.: 'Attenuation and radiation characteristics of the HE_{11}- mode.' *IEEE Trans. Microwave Theory and Tech.*, Vol. MTT-28, No. 7, July, 1980, pp. 704-710.

* Dragone, C., "High-Frequency Behavior of Waveguides with Finite Surface Impedances." *B. S. T. J.*, Vol. 60, No. 1, January 1981, pp. 89-116.

* Elsherbeni, A.Z., J. Stanier and M. Hamid; "Eigenvalues of Propagating Waves in a Circular Waveguide with an Impedance Wall", *Submitted for Publication, Aug. 1986.*

* Felsen, L.B., 'Electromagnetic properties of wedge and cone surfaces with a linearly varying surface impedance' *IRE Trans. Ant. Prop.*, AP-7, Special Supplement, 1959, pp. s231-s243.

* Hamid, M., Bhartia, P., Mohsen, A., Boerner, and W.M., Boulanger, R.J.: 'Diffraction by dielectric-loaded conical horn antennas.' European Microwave Conference, London, 1969, pp. 363-365.

* Hadidi, A.: 'Eigenvalues of dielectric-coated conical structures.' M.Sc. thesis, University of Manitoba, Canada, 1985.

* Harrington, R.F., **Time-Harmonic Electromagnetic Fields,** McGraw-Hill Book Co., New York, 1961.

* International Mathematical and Statistical Library, Problem-solving Software System for Mathematical and Statistical Fortran programming, 1984.

* Jeuken, M.E.J.; "Experimental radiation patterns of the corrugated conical-horn antenna with wide flare-angle", *Electron. Lett.*, 1969, No. 5, pp. 484-485.

* Jones, E.M.T.; "Paraboloid Reflector and Hyperboloid Lens Antennas", *IRE Trans.*, AP-2, July 1954, pp 119-127.

* Karbowiak, A.E., "Theory of Imperfect Waveguides: The Effect of Wall Impedance"; *Proc. IEE*, Vol. 102, September 1955, pp. 698-708.

* Kay, A.F.; "The Wide Flare Horn- A Novel Feed for Low Noise Broadband and High Aperture Efficiency Antennas", *Technical Research Group*, Scientific Report No. 2, Contract No. AFCRL-62-757, October 2, 1962, pp. 31.

* Kay, A.F.; "The Scalar Feed", AFCRL REP 64-3471, AD 601 609, March 1964.

* Knop, C.M., Y.B. Cheng and E.L. Ostertag; "On the Fields in a Conical Horn having an Arbitrary Wall Impedance", *IEEE Trans. Ant. Prop.*, Vol. AP-34, No. 9, September 1986, pp. 1092-1098.

* Lawrie, R.E. and L. Peters Jr.; "Modifications of Horn Antennas for Low Sidelobe Levels", *IEEE Trans. Ant. Prop.* Vol. AP-14, September 1966, pp 605-610.

* Leontovich, M.A., *Investigations of Propagation of Radiowaves, Part II.* Moscow, 1948.

* Lewin, L.; **Theory of Waveguides** Halsted Press, Butterworth and Co., London, 1975.

* Lier, E.: "A Dielectric Hybrid Mode Antenna Feed: a Simple Alternative to the Corrugated Horn." *Proc. IEEE. Trans. Ant. Prop.*, Vol. AP-34, No. 1, January 1986,pp. 21-29.

* Lier, E. and Aas, J.A.; "Simple hybrid mode horn feed loaded with a dielectric cone" *Elec. Lett.*, Vol. 21,No. 13,June 20,1985,pp. 563-564.

* Love, A.W.; "Hybrid Mode Feeds", Invited Paper, ANTEM Conference, University of Manitoba, Winnipeg, Canada, August 1986.

* Ludwig, A.C.; "The definition of cross polarization." *Proc. IEEE. Trans. Ant. Prop.*, Vol. AP-21, January 1973,pp. 116-119.

* Minnett, H.C. and Thomas, B.MacA., "A Method of Synthesizing Radiation Patterns with Axial Symmetry." *IEEE Trans. Ant. Prop.*, Vol. AP-14, September 1966, pp. 654-656.

* Minnett, H.C. and Thomas, B.MacA.; "Horn Antennas with Uniform Power Patterns Around Their Axes"; *Proc. IEEE. Trans. Ant. Prop.*, Vol. AP-14, No. 9, September 1966,pp. 656-658.

* Mohsen, A. and Hamid, M.A.K., "Wave Propagation in a Circular Waveguide with an Absorbing Wall", *J. Appl. Phys.* Vol. 41, No. 1, January 1970, pp. 433-434.

* Nagelberg, E.R.; "Phase Progression in Conical Waveguides", *B.S.T.J.*, Dec. 1967, p 2453.

* Narasimhan, M.S. and B.V. Rao; "Transmission Properties of Electromagnetic Waves in Conical Waveguides", *Int. J. Electronics*, Vol. 27, No. 2, 1969, pp. 119-138.

* Narasimhan, M.S.: "Eigenvalues of spherical hybrid modes in corrugated conical horns." *Proc. IEE*, No. 120, 1973, pp. 965-967.

* Papadopoulos, V.M., "Propagation of Electromagnetic Waves in Cylindrical Waveguides with Imperfectly Conducting Walls"; *Quart. J. Mech. and Applied Math.* Vol. VII, Pt. 3, 1954, pp. 326-334.

* Potter, P.D.; "A New Horn Antenna with Suppressed Sidelobes and Equal Beamwidths." *Microwave J.* Vol. VI, June 1963, pp. 71-78.

* Rao, K.S.; "Analysis of the Radiation Characteristics of Partially Dielectric Loaded Conical Horns", *Montech 86*, Proceedings of Conf. on Ant. and Comm., Montreal 1986, pp. 135-138.

* Rudge, A.W., K. Milne, A.D. Olver and P. Knight; **The Handbook of Antenna Design, Vol. 1,** Peter Peregrinus, London, 1982.

* Rudge, A.W. and M.J. Withers; "Design of Flared-horn Primary Feeds for Reflector Antennas", *Proc. IEE*, 117, Sept. 1970, pp. 1741-1749.

* Rumsey, V.H.; "Horn antennas with uniform power patterns around their axes." *IEEE Trans. Ant. Prop.* AP-14, 1966, pp. 656-658.

* Rumsey, V.H.; "A New Way of Solving Maxwell's Equations"; *IRE Trans. Ant. Prop.* Vol. AP-9, September 1961,pp. 461-465.

* Satoh, T.: "Dielectric loaded horn antenna.' *IEEE Trans. Ant. Prop.*, Vol. AP-20, No. 3, March 1972, pp. 199-201.

* Schelkunoff, S.A.; **Electromagnetic Waves,** D. Van Nostrand Company Inc., Princeton, N.J., 1943.

* Schorr, M.G. and Beck, F.J.; "Electromagnetic field of a conical horn". *J. Appl. Phys.* Vol. 21, Aug. 1950, pp. 795-801.

* Senior, T.B.A.; "A note on impedance boundary conditions". *Can. J. Phys.* Vol. 40, 1962, pp. 663-665.

* Silver, S; **Microwave Theory and Design.** M.I.T. Radiation Lab. Series, Vol. 12, McGraw-Hill, U.S., 1949.

* Simmons, A.J. and A.F. Kay; "The Scalar Feed; A High Performance Feed for Large Paraboloid Reflectors", *Design and Construction of Large Steerable Aerials.*, IEE Conf. Publ. 21, 1966, pp. 213-217.

* Stanier, J.D. and M. Hamid; "Hybrid Modes in a Dielectric Lined Conical Waveguide", *Electron. Lett.*, Vol. 22, No. 12, June 5, 1986, pp. 626-627.

* Thomas, B.MacA.; "Mode Conversion Using Circumferentially Corrugated Cylindrical Waveguide", *Electron. Lett.*, Vol. 8, No. 15, July 27, 1972, pp. 394-396.

* Turrin, R.H.; "Dual mode small-aperture antennas". *IEEE Trans. Ant. Prop.* AP-15, March 1967, pp. 307-308.

* Wait, J.R.; **Electromagnetic Waves in Stratified Media.** Pergammon Press, New York, 1962.

* Waldron, R.A.; **Theory of Guided Electromagnetic Waves,** London, Van Nostrand,1969.

* Weston, V.H.; "Theory of Absorbers in Scattering"; *IEEE Trans. Ant. Prop.* September 1963, pp. 576-584.

* Wong, M.N. and Brandt, C.J.; "Conical Horn Antenna Having a Mode Generator", *United States Patent no. 4,141,015.*, February 20, 1979.